



#### Available online at www.sciencedirect.com

# **ScienceDirect**

Comput. Methods Appl. Mech. Engrg. 370 (2020) 113249

Computer methods in applied mechanics and engineering

www.elsevier.com/locate/cma

# A high-order numerical approach with Cartesian meshes for modeling of wave propagation and heat transfer on irregular domains with inhomogeneous materials

A. Idesman\*, B. Dey

Department of Mechanical Engineering, Texas Tech University, Lubbock, TX 79409-1021, USA
Received 27 March 2020; received in revised form 25 June 2020; accepted 26 June 2020
Available online xxxx

#### Abstract

Recently we have developed a new numerical approach for PDEs with constant coefficients on irregular domains and Cartesian meshes. In this paper we extend it to a much more general case of PDEs with variable coefficients that have a lot of applications; e.g., the modeling of functionally graded materials, the inhomogeneous materials obtained by 3-D printing and many others. Here, we consider the 2-D wave and heat equations for isotropic and anisotropic inhomogeneous materials. The idea of the extension to the case of PDEs with variable coefficients is based on the representation of the stencil coefficients as functions of the mesh size. This leads to the increase in the size of the local system of algebraic equations solved for each grid point of the new approach; however, this does not change the size of the global system of semidiscrete equations and practically does not increase the computational costs of the proposed technique. Similar to our previous technique, the new 2-D approach with compact 9-point stencils uses trivial Cartesian meshes for complex irregular domains and provides the fourth order of accuracy for the wave and heat equations with variable coefficients. The calculation of the coefficients of the stencil equations is based on the minimization of the local truncation error of the stencil equations and yields the optimal order of accuracy of the new technique. At similar 9-point stencils, the accuracy of the new approach is much higher than that for the linear finite elements. The numerical results for irregular domains show that at the same number of degrees of freedom, the new approach is even much more accurate than the high-order (up to the third order) finite elements with much wider stencils. The wave and heat equations are uniformly treated with the new approach. © 2020 Elsevier B.V. All rights reserved.

Keywords: Wave and heat equations with variable coefficients; Functionally graded materials; Irregular domains; Cartesian meshes; Optimal accuracy

#### 1. Introduction

The finite element method, the finite volume method, the isogeometric elements, the spectral elements and similar techniques represent very powerful tools for the solution of partial differential equations (PDEs) for a complex geometry. However, the generation of non-uniform meshes for a complex geometry is not simple and may lead to the decrease in accuracy of these techniques if 'bad' elements (e.g., elements with small angles) appear in the

E-mail address: alexander.idesman@ttu.edu (A. Idesman).

Corresponding author.

mesh. Moreover, the conventional derivation of discrete equations for these techniques (e.g., based on the Galerkin approaches) does not lead to the optimal accuracy. For example, in [1–28] it has been shown that at the same form of the stencil equations of a discrete or semi-discrete system, the accuracy of the conventional finite elements and the isogeometric elements used for wave propagation can be significantly improved on regular rectangular domains with uniform meshes. This improvement is based on the analysis of the numerical dispersion error and is limited to the wave equations with constant coefficients, zero loading term and rectangular domains.

There are a significant number of publications related to the numerical solution of different PDEs on irregular domains with uniform embedded meshes. For example, we can mention the following fictitious domain numerical methods that use uniform embedded meshes: the embedded finite difference method, the cut finite element method, the finite cell method, the Cartesian grid method, the immersed interface method, the virtual boundary method, the embedded domain method, etc.; e.g., see [29–59] and many others. However, the development of numerical techniques for the solution of complex PDEs on irregular domains with optimal accuracy is still a challenging problem (e.g., see [60]).

Recently in our papers [61–66] we have developed a new numerical technique for the solution of PDEs with constant coefficients on regular and irregular domains with Cartesian meshes. We called this approach the optimal local truncation error method (OLTEM); see [61,62]. At the same structure of the semidiscrete or discrete equations, the new technique provides the optimal order of accuracy that exceeds the order of accuracy of many known numerical approaches on regular and irregular domains. Here, we extend it to a much more general case of PDEs with variable coefficients that have a lot of engineering applications; e.g., the modeling of functionally graded materials, the inhomogeneous materials obtained by 3-D printing and many others. In this paper, we consider the 2-D isotropic and anisotropic wave and heat equations with variable coefficients on irregular domains and Cartesian meshes.

Wave propagation in an anisotropic inhomogeneous medium is described by the following scalar wave equation in domain  $\Omega$ :

$$\frac{\partial^2 u}{\partial t^2} - \left[ \frac{\partial}{\partial x} \left( c_x^2(x, y) \frac{\partial u}{\partial x} \right) + \frac{\partial}{\partial y} \left( c_y^2(x, y) \frac{\partial u}{\partial y} \right) \right] = f. \tag{1}$$

Similarly, the heat equation in domain  $\Omega$  can be written as:

$$\frac{\partial u}{\partial t} - \left[ \frac{\partial}{\partial x} \left( a_x(x, y) \frac{\partial u}{\partial x} \right) + \frac{\partial}{\partial y} \left( a_y(x, y) \frac{\partial u}{\partial y} \right) \right] = f.$$
 (2)

In Eqs. (1)–(2),  $c_x$  and  $c_y$  are the wave velocity along the x- and y-axes ( $c_x = c_y$  for isotropic materials),  $a_x$  and  $a_y$  are the thermal diffusivity along the x- and y-axes ( $a_x = a_y$  for isotropic materials),  $f(\mathbf{x}, t)$  is the loading or source term, u is the field variable. The Dirichlet boundary conditions  $u = g_1$  are applied along the boundary  $\Gamma$ . The initial conditions are  $u(\mathbf{x}, t = 0) = g_2$ ,  $v(\mathbf{x}, t = 0) = g_3$  in  $\Omega$  for the wave equation and  $u(\mathbf{x}, t = 0) = g_4$  in  $\Omega$  for the heat equation where  $g_i$  (i = 1, 2, 3, 4) are the given functions. According to the new approach, the semidiscrete system for the wave and heat equations after the space discretization with a Cartesian rectangular mesh can be represented as a system of ordinary differential equations in time. The ordinary differential equation of this system formed for each internal grid point is called the stencil equation and can be written down as follows:

$$\sum_{i=1}^{M} [h^2 \bar{m}_i(h) \frac{d^n u_i^{num}}{dt^n} + \bar{k}_i(h) u_i^{num}] = \tilde{f},$$
(3)

where  $u_i^{num}$  and  $\frac{d^n u_i^{num}}{dt^n}$  are the numerical solution for function u and its time derivative at the grid points,  $\bar{m}_i(h)$  and  $\bar{k}_i(h)$  are the unknown coefficients to be determined,  $\tilde{f}(t)$  is the discretized loading (source) term (see the next sections), M is the number of the grid points included into the stencil equation, n=2 for the wave equation and n=1 for the heat equation, h is the mesh size along the x-axis. In contrast to our approach presented in [61–63] for the wave (heat) equation with constant coefficients, now we assume that the coefficients  $\bar{m}_i(h)$  and  $\bar{k}_i(h)$  depend on h. Many numerical techniques such as the finite difference method, the finite element method, the finite volume method, the isogeometric elements, the spectral elements, different meshless methods and others can be finally reduced to Eq. (3) with some specific coefficients  $\bar{m}_i$  and  $\bar{k}_i$  for the wave and heat equations. In the derivations below, we will assume 9-point stencils (M=9) in the 2-D case that are similar to the 9-point stencils of the linear

quadrilateral finite elements on Cartesian meshes. Generally, the stencils with any number of points M can be used with the suggested approach.

Let us introduce the local truncation error used with the new approach. The replacement of the numerical values of function  $u_i^{num}$  and its time derivatives  $\frac{d^n u_i^{num}}{dt^n}$  at the grid points in Eq. (3) by the exact solution  $u_i$  and  $\frac{d^n u_i}{dt^n}$  to the wave or heat equation, Eqs. (1) or (2), leads to the residual e of this equation called the local truncation error of the semidiscrete equation, Eq. (3):

$$e = \sum_{i=1}^{M} [h^2 \bar{m}_i(h) \frac{d^n u_i}{dt^n} + \bar{k}_i(h) u_i] - \tilde{f}.$$
(4)

Calculating the difference between Eqs. (4) and (3) we can get

$$e = \sum_{i=1}^{M} \{h^2 \bar{m}_i(h) \left[ \frac{d^n u_i}{dt^n} - \frac{d^n u_i^{num}}{dt^n} \right] + \bar{k}_i(h) \left[ u_i - u_i^{num} \right] \} = \sum_{i=1}^{M} \left[ h^2 \bar{m}_i(h) \bar{e}_i^v + \bar{k}_i(h) \bar{e}_i^u \right], \tag{5}$$

where  $\bar{e}_i^u = u_i - u_i^{num}$  and  $\bar{e}_i^v = \frac{d^n u_i}{dt^n} - \frac{d^n u_i^{num}}{dt^n}$  are the errors of function u and its time derivatives at the grid points i. As can be seen from Eq. (5), the local truncation error e is a linear combination of the errors of the function u and its time derivatives at the grid points i which are included into the stencil equation.

In Section 2 a new numerical approach with 9-point uniform and nonuniform stencils is uniformly derived for the 2-D wave and heat equations with variable coefficients and zero and non-zero loading (source) term. The new 2-D approach with compact 9-point stencils provides the fourth order of accuracy for the wave and heat equations with variable coefficients. The calculation of the coefficients of the stencil equations is based on the minimization of the local truncation error of the stencil equations and yields the optimal order of accuracy of the new technique. At similar 9-point stencils, the accuracy of the new approach is much higher than that for the linear finite elements. Numerical examples on regular and irregular domains as well as the comparison with FEM are presented in Section 3. The numerical results for irregular domains show that at the same number of degrees of freedom, the new approach is even much more accurate than the high-order (up to the third order) finite elements with much wider stencils. For the derivation of many analytical expressions presented below we use the computational program "Mathematica" (see [67]).

## 2. A new numerical approach for the 2-D wave and heat equations with variable coefficients

#### 2.1. Zero load (source) term f = 0 in Eqs. (1) and (2)

Here, we present 9-point uniform stencils that will be used for the internal grid points located far from the boundary and 9-point non-uniform stencils that will be used for the grid points located close to the boundary. Let us consider a 2-D bounded domain and a Cartesian rectangular mesh with a mesh size h where h is the size of the mesh along the x-axis,  $b_y h$  is the size of the mesh along the y-axis ( $b_y$  is the aspect ratio of the mesh); see Figs. 1 and 2. The 9-point uniform stencil considered here is similar to that for the 2-D linear quadrilateral finite elements. The spatial locations of the 8 degrees of freedom that are close to the internal degree of freedom  $u_5$  and contribute to the 9-point uniform stencil for this degree of freedom are shown in Fig. 1 for the case when the boundary and the Cartesian mesh are matched or when the degree of freedom  $u_5$  is located far from the boundary. In the case of non-matched grids when the grid points do not coincide with the boundary and the 9-point uniform stencil for an internal point  $u_5$  in Fig. 1 is not possible due to the location of some grid points of the Cartesian mesh outside the physical domain, we use the following procedure for the formation of the 9-point nonuniform stencil. In order to find the boundary points that are included into the 9-point non-uniform stencil for the degree of freedom  $u_5$  (see Fig. 2) we join the central point u<sub>5</sub> with the 8 closest grid points; i.e., we have eight straight lines along the x- and y-axes and along the diagonal directions (the dashed lines) of the grid; see Fig. 2. If any of these lines intersect the boundary of the domain then the corresponding regular grid points (designated as o in Fig. 2) are moved to the boundary (the location of these boundary points in Fig. 2 is designated as •). This means that for all internal grid points located within the domain we use a 9-point uniform (see Fig. 1) or non-uniform (see Fig. 2) stencil with 9 points totally (regular grid points and the boundary points). For convenience, the local numeration of the grid points from 1 to 9 is used in Figs. 1 and 2 as well as in the derivations below for the 9-point uniform and

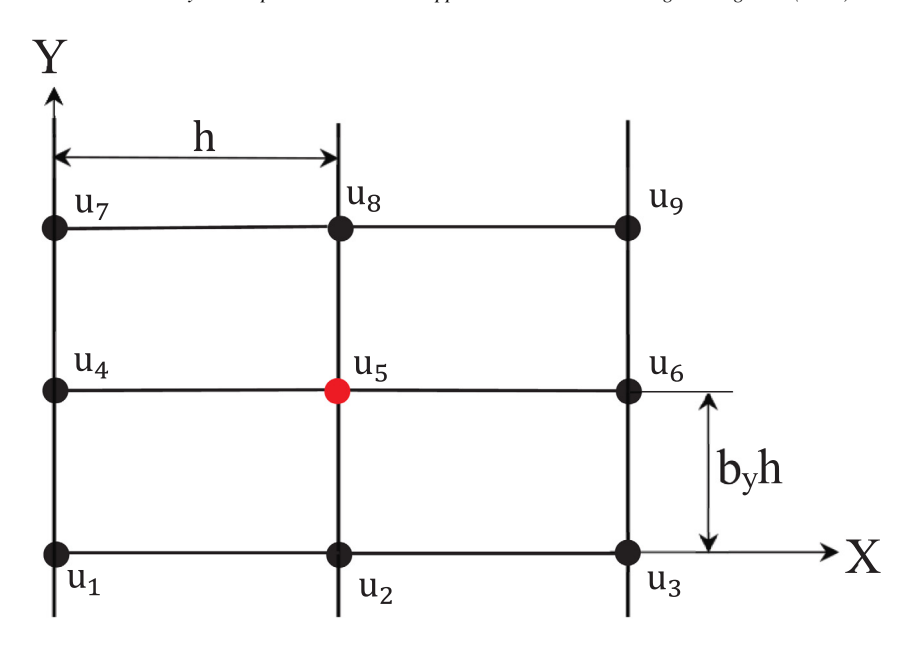


Fig. 1. The spatial locations of the degrees of freedom  $u_p$  (p = 1, 2, ..., 9) contributing to the 9-point uniform stencil for the internal degree of freedom  $u_5$  located far from the boundary.

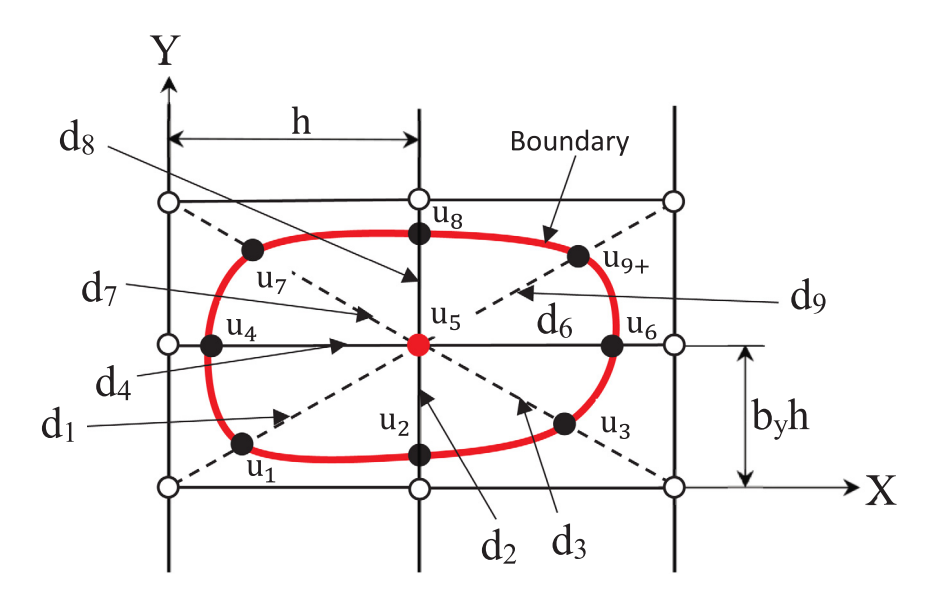


Fig. 2. The spatial locations of the degrees of freedom  $u_p$  (p = 1, 2, ..., 9) that contribute to the 9-point nonuniform stencil for the internal degree of freedom  $u_5$  located close to the boundary.

non-uniform stencils. To describe the coordinates of the boundary points for non-uniform stencils (see Fig. 2) we introduce 9 coefficients  $0 \le d_p \le 1$  (p = 1, 2, ..., 9) as follows (see also Fig. 2):

$$x_p = x_5 + (i-2)d_p h$$
,  $y_p = y_5 + (j-2)d_p b_y h$ , (6)

where  $d_5 = 0$ , p = 3(j - 1) + i with i, j = 1, 2, 3. Eq. (6) can be also used for the coordinates of the grid points inside the domain with the corresponding coefficients  $d_p$  equal to unity  $(d_p = 1)$ .

Eq. (3) for the 9-point uniform (see Fig. 1) or nonuniform (see Fig. 2) stencil for the grid point  $u_5$  will be assumed in the following form:

$$h^{2} \sum_{p=1}^{9} (m_{0,p} + m_{1,p}h) \frac{d^{n} u_{p}^{num}}{dt^{n}} + \sum_{p=1}^{9} (k_{0,p} + k_{1,p}h + k_{2,p}h^{2} + k_{3,p}h^{3} + k_{4,p}h^{4}) u_{p}^{num} = \bar{f}_{5},$$
 (7)

where  $\bar{f}_5 = 0$  in the case of zero load (source) f = 0 in Eqs. (1) and (2), the 63 unknown stencil coefficients  $m_{i,p}$ ,  $k_{j,p}(i=0,1,j=0,1,2,3,4,p=1,2,\ldots,9)$  are to be determined from the minimization of the local truncation error, the superscript n in the time derivative in Eq. (7) is n=1 for the heat equation and n=2 for the wave equation. The stencil equation, Eq. (7), can be written in the form similar to that for the wave (heat) equation with constant coefficients:

$$h^2 \sum_{p=1}^{9} \bar{m}_p(h) \frac{d^n u_p^{num}}{dt^n} + \sum_{p=1}^{9} \bar{k}_p(h) u_p^{num} = \bar{f}_5,$$
 (8)

with  $\bar{m}_p(h) = m_{0,p} + m_{1,p}h$  and  $\bar{k}_p(h) = k_{0,p} + k_{1,p}h + k_{2,p}h^2 + k_{3,p}h^3 + k_{4,p}h^4$  (p = 1, 2, ..., 9) where the 18 coefficients  $\bar{m}_p(h)$  and  $\bar{k}_p(h)$  are the polynomial functions of the mesh size h (for the wave and heat equations with constant coefficients, the coefficients  $\bar{m}(h)_p$  and  $\bar{k}(h)_p$  are constant and independent of h; i.e.,  $\bar{m}_p(h) = m_{0,p}$  and  $\bar{k}_p(h) = k_{0,p}$ ). This polynomial representation of  $\bar{m}_p(h)$  and  $\bar{k}_p(h)$  can be considered as a Taylor series of functions  $\bar{m}_p(h)$  and  $\bar{k}_p(h)$ .

Remark 1. Only 62 out of the 63 coefficients  $m_{i,p}$ ,  $k_{j,p}(i=0,1,j=0,1,2,3,4,p=1,2,...,9)$  in Eq. (7) can be considered as unknown coefficients. This can be explained as follows. In the case of zero load f=0 and  $\bar{f}_5=0$ , Eq. (8) can be rescaled by the division of the left and right sides of Eq. (7) by any scalar  $a_1$ ; i.e., one of the coefficients can be selected as unity and there will be only 62 unknown rescaled coefficients. The case of nonzero load  $\bar{f}_5 \neq 0$  can be similarly treated because the term  $\bar{f}_5$  is a linear function of the stencil coefficients; see below. For convenience, we will scale the stencil coefficients in such a way that for any h the coefficient  $\bar{k}_5(h)$  is  $\bar{k}_5(h)=1$ .

The local truncation error e of the stencil equation, Eq. (8), at any time t can be written down by the replacement of the numerical solution in Eq. (8) by the exact solution as follows:

$$e = h^2 \sum_{p=1}^{9} \bar{m}_p(h) \frac{\partial^n u_p}{\partial t^n} + \sum_{p=1}^{9} \bar{k}_p(h) u_p - \bar{f}_5,$$
(9)

where function u(x, y, t) in Eq. (9) corresponds to the exact solution. In order to represent the local truncation error e as a Taylor series, let us expand the exact solution and the time derivative of the exact solution in Eq. (9) into a Taylor series at small  $h \ll 1$  as follows:

$$u_{p} = u_{5} + \frac{\partial u_{5}}{\partial x} [(i-2)d_{p}h] + \frac{\partial u_{5}}{\partial y} [(j-2)d_{p}b_{y}h] + \frac{\partial^{2}u_{5}}{\partial x^{2}} \frac{[(i-2)d_{p}h]^{2}}{2!} + \frac{\partial^{2}u_{5}}{\partial y^{2}} \frac{[(j-2)d_{p}b_{y}h]^{2}}{2!} + 2\frac{\partial^{2}u_{5}}{\partial x\partial y} \frac{[(i-2)d_{p}h][(j-2)d_{p}b_{y}h]}{2!} + \cdots,$$
(10)

$$\frac{\partial^{n} u_{p}}{\partial t^{n}} = \frac{\partial^{2} u_{5}}{\partial t^{n}} + \frac{\partial^{n+1} u_{5}}{\partial t^{n} \partial x} [(i-2)d_{p}h] + \frac{\partial^{n+1} u_{5}}{\partial t^{n} \partial y} [(j-2)d_{p}b_{y}h] + \frac{\partial^{n+2} u_{5}}{\partial t^{n} \partial x^{2}} \frac{[(i-2)d_{p}h]^{2}}{2!} + \frac{\partial^{n+2} u_{5}}{\partial t^{n} \partial y^{2}} \frac{[(j-2)d_{p}b_{y}h]^{2}}{2!} + 2 \frac{\partial^{n+2} u_{5}}{\partial t^{n} \partial x \partial y} \frac{[(i-2)d_{p}h][(j-2)d_{p}b_{y}h]}{2!} + \cdots,$$
(11)

where p = 3(j-1) + i with i, j = 1, 2, 3; see Fig. 2. The exact solution  $u_5$  to the wave and heat equations, Eqs. (1) and (2), at  $x = x_5$  and  $y = y_5$  meets the following equations:

$$\frac{\partial^n u_5}{\partial t^n} - \left[ \frac{\partial}{\partial x} \left( \bar{c}_x(x, y) \frac{\partial u}{\partial x} \right) + \frac{\partial}{\partial y} \left( \bar{c}_y(x, y) \frac{\partial u}{\partial y} \right) \right]_{|x = x_5, y = y_5} = f_5,$$
(12)

$$\frac{\partial^{(i+j+n)} u_5}{\partial t^n \partial x^i \partial y^j} - \left[ \frac{\partial^{(i+j+1)}}{\partial x^{(i+1)} \partial y^j} \left( \bar{c}_x(x, y) \frac{\partial u}{\partial x} \right) + \frac{\partial^{(i+j+1)}}{\partial x^i \partial y^{(j+1)}} \left( \bar{c}_y(x, y) \frac{\partial u}{\partial y} \right) \right]_{|x=x_5|, y=y_5} = \frac{\partial^{(i+j)} f_5}{\partial x^i \partial y^j}, \tag{13}$$

with  $\bar{c}_x = c_x^2$  and  $\bar{c}_y = c_y^2$  for the wave equation,  $\bar{c}_x = a_x$  and  $\bar{c}_y = a_y$  for the heat equation as well as  $u_5 = u(x = x_5, y = y_5, t)$  and  $i, j = 0, 1, 2, 3, 4, \ldots$ , the derivatives of the functions  $u, \bar{c}_x$  and  $\bar{c}_y$  in Eqs. (12) and (13) are calculated at the central grid point of the stencil with the coordinates  $x = x_5$  and  $y = y_5$ . Here, Eq. (13) is directly obtained by the differentiation of Eq. (12) with respect to x and y. Inserting Eqs. (10)–(11) and Eqs. (12)–(13) and with zero loading term f = 0 into Eq. (9) we will get the following local truncation error in space e:

$$e = \bar{c}\{b_{1}u_{5} + h[b_{2}\frac{\partial u_{5}}{\partial x} + b_{3}\frac{\partial u_{5}}{\partial y} + b_{4}u_{5}] + h^{2}[b_{5}\frac{\partial^{2}u_{5}}{\partial x^{2}} + b_{6}\frac{\partial^{2}u_{5}}{\partial x\partial y} + b_{7}\frac{\partial u_{5}}{\partial x} + b_{8}\frac{\partial^{2}u_{5}}{\partial y^{2}} + b_{9}\frac{\partial u_{5}}{\partial y} + b_{10}u_{5}]$$

$$+h^{3}[b_{11}\frac{\partial^{3}u_{5}}{\partial x^{3}} + \dots + b_{20}u_{5}] + h^{4}[b_{21}\frac{\partial^{4}u_{5}}{\partial x^{4}} + \dots + b_{35}u_{5}] + h^{5}[b_{36}\frac{\partial^{5}u_{5}}{\partial x^{5}} + \dots + b_{56}u_{5}]$$

$$+h^{6}[b_{57}\frac{\partial^{6}u_{5}}{\partial x^{6}} + \dots + b_{84}u_{5}] + h^{7}[b_{85}\frac{\partial^{7}u_{5}}{\partial x^{7}} + \dots + b_{120}u_{5}] + h^{8}[b_{121}\frac{\partial^{8}u_{5}}{\partial x^{8}} + \dots + b_{165}u_{5}]\}$$

$$+O(h^{9}),$$

$$(14)$$

where the coefficients  $b_p$  (p = 1, 2, ...) are expressed in terms of the coefficients  $m_{i,p}$ ,  $k_{j,p}$  (i = 0, 1, j = 0, 1, 2, 3, 4, p = 1, 2, ..., 9); see Appendix A for the detailed expression of Eq. (14) and the coefficients  $b_p$ . We should mention that by the use of the wave (heat) equation, Eqs. (12)–(13), the time derivatives in Eq. (14) for the local truncation error are excluded.

For the uniform stencil in Fig. 1 with  $d_p = 1$  (p = 1, 2, ..., 9) the expressions for coefficients  $b_p$  (p = 1, 2, ...) are simplified and some results can be analytically obtained. For example, equating to zero coefficients  $b_p = 0$  ( $p = 1, 2, ..., 26, 28, ..., 35, 37, ..., 41, 43, 44, 45, 48, 49, 50, 54, 55, 60, 61, 64, 70, 71, 75, 76, 82, 93, 104, 110) and using the scaling equations <math>k_{0,5} = 1$  and  $k_{1,5} = k_{2,5} = k_{3,5} = k_{4,5} = 0$  we can get 63 algebraic equations with the 63 unknown stencil coefficients  $m_{i,p}$ ,  $k_{j,p}$  (i = 0, 1, j = 0, 1, 2, 3, 4, p = 1, 2, ..., 9). Solving this system of equations we can analytically find the 63 unknown stencil coefficients  $m_{i,p}$ ,  $k_{j,p}$ ; see Appendix B. Because some of the coefficients  $b_p$  for the fourth and fifth order terms in Eq. (14) are linear dependent, the analytical solution given in Appendix B zeros the first 56 coefficients  $b_p$  in Eq. (14); i.e., for uniform stencils we can get the sixth order of the local truncation error in Eq. (14) (see Appendix B).

In order to improve the order of the local truncation error in Eq. (14) for non-uniform stencils at small  $h \ll 1$ , the following procedure can be suggested. First, we will zero the first 20 coefficients  $b_p$  in Eq. (14) up to the third order with respect to h; i.e.,

$$b_p = 0, p = 1, 2, \dots, 20.$$
 (15)

Then, in order to have a sufficient number of equations for the calculation of the 63 stencil coefficients  $m_{i,p}$ ,  $k_{j,p}$  (i = 0, 1, j = 0, 1, 2, 3, 4, p = 1, 2, ..., 9), we use the least square method for the minimization of coefficients  $b_p$  related to the fourth and higher orders of the local truncation error with the following residual R:

$$R = \sum_{p=21}^{35} b_p^2 + h_1 \sum_{p=36}^{56} b_p^2 + h_2 \sum_{p=57}^{84} b_p^2 + h_3 \sum_{p=85}^{120} b_p^2 + h_4 \sum_{p=121}^{165} b_p^2,$$
 (16)

where  $h_i$  (i = 1, 2, 3, 4) are the weighting factors to be selected (e.g., the numerical experiments show that  $h_i = 0.1$  (i = 1, 2, 3, 4) yields accurate results). In order to minimize the residual R with the constraints given by Eq. (15) and the scaling equation  $\bar{k}_5(h) = k_{0,5} + k_{1,5}h + k_{2,5}h^2 + k_{3,5}h^3 + k_{4,5}h^4 = 1$ , we can form a new residual  $\bar{R}$  with the Lagrange multipliers  $\lambda_p$ :

$$\bar{R} = \sum_{l=1}^{20} \lambda_l b_l + \lambda_{21} (\bar{k}_5(h) - 1) + \sum_{p=21}^{35} b_p^2 + h_1 \sum_{p=36}^{56} b_p^2 + h_2 \sum_{p=57}^{84} b_p^2 + h_3 \sum_{p=85}^{120} b_p^2 + h_4 \sum_{p=121}^{165} b_p^2.$$
 (17)

The residual  $\bar{R}$  is a quadratic function of coefficients  $m_{i,p}$ ,  $k_{j,p}$  ( $i=0,1,\ j=0,1,2,3,4,\ p=1,2,\ldots,9$ ) and a linear function of the Lagrange multipliers  $\lambda_l$ ; i.e.,  $R=R(m_{i,p},k_{j,p},\lambda_l)$ . In order to minimize the residual

 $\bar{R} = \bar{R}(m_{i,p}, k_{j,p}, \lambda_l)$ , the following equations based on the least square method for the residual  $\bar{R}$  can be written down:

$$\frac{\partial \bar{R}}{\partial m_{i,p}} = 0, \qquad \frac{\partial \bar{R}}{\partial k_{j,p}} = 0, \qquad \frac{\partial \bar{R}}{\partial \lambda_l} = 0, 
i = 0, 1, 2, \qquad j = 0, 1, 2, 3, 4, \qquad p = 1, 2, \dots, 9, \qquad l = 1, 2, \dots, 21.$$
(18)

Eq. (18) forms a system of 84 linear algebraic equations with respect to 63 unknown coefficients  $m_{i,p}$ ,  $k_{j,p}$  (i = 0, 1, j = 0, 1, 2, 3, 4, p = 1, 2, ..., 9) and 21 Lagrange multipliers  $\lambda_l$  (l = 1, 2, ..., 21). Solving these linear algebraic equations numerically, we can find the coefficients  $m_{i,p}$ ,  $k_{j,p}$  (i = 0, 1, j = 0, 1, 2, 3, 4, p = 1, 2, ..., 9) for the 9-point non-uniform stencils. Numerical experiments show that for small weighting coefficients  $h_i$  (i = 1, 2, 3, 4), the minimization of the residual  $\bar{R}$  in Eq. (17) leads to very small coefficients  $b_p$  (p = 21, ..., 35) of the leading terms related to the fourth order of the local truncation error; i.e., the presented procedure provides the fifth order of the local truncation error for the 9-point non-uniform stencils and the sixth order of the local truncation error for the 9-point uniform stencils with the stencil coefficients given in Appendix B. This leads to the fourth order of accuracy of global solutions; see the numerical examples below. Moreover, due to the minimization of the leading fifth order terms of the local truncation error in Eq. (17) for nonuniform stencils, at the same numbers of degrees of freedom the new approach on irregular domains yields more accurate results than those obtained by the high-order finite elements (up to the third order) with much wider stencils; see the numerical examples below.

**Remark 2.** We do not include the equations for coefficients  $b_p$  ( $p=21,\ldots,35$ ) as constraints  $b_p=0$  ( $p=21,\ldots,35$ ) in Eq. (17) because as mentioned before, some of the coefficients  $b_p$  ( $p=21,\ldots,35$ ) are linear dependent.

**Remark 3.** We should also mention that the inclusion of more boundary points into the stencil equation, Eq. (3), does not increase the width of the global system of equations (due to the imposition of the boundary conditions at these points) but can lead to the accuracy improvement. This will be studied in the future.

Remark 4. To estimate the computation costs of the solution of 84 linear algebraic equations formed by Eq. (18) we solved  $10^6$  such systems with a general MATLAB solver on a simple student laptop computer (Processor: Intel (R) Core(TM) i5-4210U CPU @ 1.70 GHz 2.40 GHz). The computation 'wall' time was T = 7356 s for  $10^6$  systems or the average time for one system was 0.007356 s. Because the coefficients  $m_{i,p}$ ,  $k_{j,p}$  (i = 0, 1, j = 0, 1, 2, 3, 4, p = 1, 2, ..., 9) are independently calculated for different non-uniform stencils, the computation time of their calculation for different grid points can be significantly reduced on modern parallel computers. This means that for large global systems of equations, the computation time for the calculation of the coefficients  $m_{i,p}$ ,  $k_{j,p}$  (i = 0, 1, j = 0, 1, 2, 3, 4, p = 1, 2, ..., 9) is very small compared to that for the solution of the global system of equations. We should mention that the Lagrange multipliers  $\lambda_l$  in the local system of equations, Eq. (18), are only used for the calculation of the 63 unknown coefficients  $m_{i,p}$ ,  $k_{j,p}$  (i = 0, 1, j = 0, 1, 2, 3, 4, p = 1, 2, ..., 9) and are not used in the global system of equations.

**Remark 5.** The proposed technique yields accurate results for the non-uniform stencils even with very small coefficients  $d_i \ll 1$ . However, the new technique permits exclusion of very small coefficients  $d_i \ll 1$  from calculations. For example, if  $d_i \ll tol$  for some internal point where tol is a small tolerance (e.g.,  $tol = 10^{-3}$ ), then the non-uniform stencil for this internal point can be removed from the global system of equations and this point can be moved to the boundary and treated as the boundary point for other stencils. In this case, the corresponding coefficients  $d_i$  for this point in other stencils can be slightly greater than one. According to the derivations in the previous section, all equations will be valid also for  $d_i > 1$ . The numerical experiments with a small tolerance  $tol = 10^{-3}$  show that if the point with very small coefficients  $d_i \ll 1$  is moved to the boundary then the coefficients  $d_i$  for this point in other stencils can be taken as  $d_i = 1$  without introducing any significant errors.

The final semi-discrete system of equations includes the 9-point uniform and nonuniform stencil equations (see Figs. 1 and 2) for all internal grid points that are located inside the domain. We should also mention that the new approach with 9-point stencils for the wave and heat equations with variable coefficients on irregular domains provides the same fourth order of accuracy as that for our approach for the wave and heat equations with constant coefficients presented in [61–63].

#### 2.2. Nonzero load (source) term $f \neq 0$ in Eqs. (1) and (2)

The inclusion of non-zero loading (source) term f in the partial differential equations, Eqs. (1) and (2), leads to the non-zero term  $\bar{f}_5$  in the stencil equation, Eq. (8) (similar to Eq. (3)). The expression for the term  $\bar{f}_5$  can be calculated from the procedure used for the derivation of the local truncation error in the case of zero loading (source) term as follows. In the case of non-zero loading (source) term  $f(\mathbf{x}, t) \neq 0$  and  $f_5 \neq 0$ , the insertion of Eqs. (10)–(11) and Eqs. (12)–(13) into Eq. (9) yields the following local truncation error in space  $e_f$ :

$$e_f = e - [\bar{f}_5 - \{h^2 f_5(m_{0.1} + m_{0.2} + m_{0.3} + \cdots) + \cdots\}], \tag{19}$$

where e is the local truncation error in space given by Eq. (14) for zero loading (source) term,  $f_5$  designates function f(x, y, t) calculated at  $x = x_5$  and  $y = y_5$ . Equating to zero the expression in the square brackets on the right-hand side of Eq. (19), we will get the expression for  $\bar{f}_5$ :

$$\bar{f}_5 = \mathbf{h}^2 f_5(m_{0,1} + m_{0,2} + m_{0,3} + \dots) + \dots, \tag{20}$$

as well as we will get the same local truncation errors  $e_f = e$  for zero and non-zero loading functions (see Appendix C for the detailed expression of  $\bar{f}_5$ ). This means that the coefficients  $m_{i,p}$ ,  $k_{j,p}$  (i = 0, 1, j = 0, 1, 2, 3, 4, p = 1, 2, ..., 9) of the stencil equations are first calculated for zero loading (source) term f = 0 as described in Section 2.1. Then, the nonzero loading (source) term  $\bar{f}_5$  given by Eq. (20) is used in the stencil equation, Eq. (8).

#### 3. Numerical examples

In this section the computational efficiency of the new approach developed in this paper will be demonstrated and compared with the 2-D conventional linear (T3 and Q4), quadratic (T6 and Q9) and cubic (T10 and Q16) quadrilateral (Q4, Q9, Q16) and triangular (T3, T6, T10) finite elements. As known (e.g., see [68]), finite elements provide the (p+1)th order of convergence where p is the order of finite elements. The commercial finite element software 'COMSOL' (see [69]) is used for the finite element simulations. Similar to the finite element terminology, a grid point of a Cartesian mesh will be called a node. In order to compare the accuracy of the new approach with FEM, the following errors are considered below. The relative errors  $e_u^i$  for the function u and  $e_v^i$  for its first time derivative at the ith node are defined as:

$$e_u^i = \frac{|u_i^{num} - u_i^{exact}|}{u_{max}^{exact}} \quad \text{and} \quad e_v^i = \frac{|v_i^{num} - v_i^{exact}|}{v_{max}^{exact}}, \quad i = 1, 2, \dots, N.$$
 (21)

The maximum relative errors  $e_u^{max}$  for the function u and  $e_v^{max}$  for its first time derivative are defined as:

$$e_u^{max} = \max_i e_u^i$$
 and  $e_v^{max} = \max_i e_v^i$ ,  $i = 1, 2, ..., N$ . (22)

In Eqs. (21)–(22) the superscripts 'num' and 'exact' correspond to the numerical and exact solutions; N is the total number of nodes used in calculations;  $u_{max}^{exact}$  and  $v_{max}^{exact}$  are the maximum absolute value of the exact solution over the entire domain for the function u and its first time derivative, respectively. The errors given by Eqs. (21)–(22) are evaluated at the final observation time T. The errors  $e_v^i$  and  $e_v^{max}$  are used for the wave equation only. For the time integration, the trapezoidal rule and the backward difference method are used for the wave and the heat equations, respectively. A sufficiently small size of time increments is used in calculations. In this case the error in time can be neglected and the numerical error corresponds to the error in space only. For convenience, the function u is called 'displacement' and 'temperature' for the wave and the heat equations, respectively.

For the test problems in the following sections, first a simple rectangular plate ABCD with the dimensions  $1 \times 2$  is considered with square  $(b_y = 1)$  Cartesian meshes; see Fig. 3. Then, the new approach is applied to a complex irregular domain presented by a trapezoidal plate OPQR with circular and quadrilateral holes; see Fig. 5a. Fig. 5 also shows a Cartesian mesh used for the new approach as well as examples of typical quadrilateral and triangular meshes generated by COMSOL for the conventional finite elements. For convenience, we generate the Cartesian mesh for the new approach by keeping one horizontal grid line matched with the edge OP and one vertical grid line matched with the edge OR; see Fig. 5. The circular and quadrilateral holes as well as the edge QR are non-matched with the mesh whereas the edge PQ can be matched or non-marched with the vertical grid line depending on the mesh size h. For the test problems solved below the observation time is chosen to be T = 0.2. The initial conditions over the entire domain at time t = 0, the Dirichlet boundary conditions along the entire boundary as well as the non-zero loading (source) term f(x, y, t) are calculated according to the selected exact solutions.

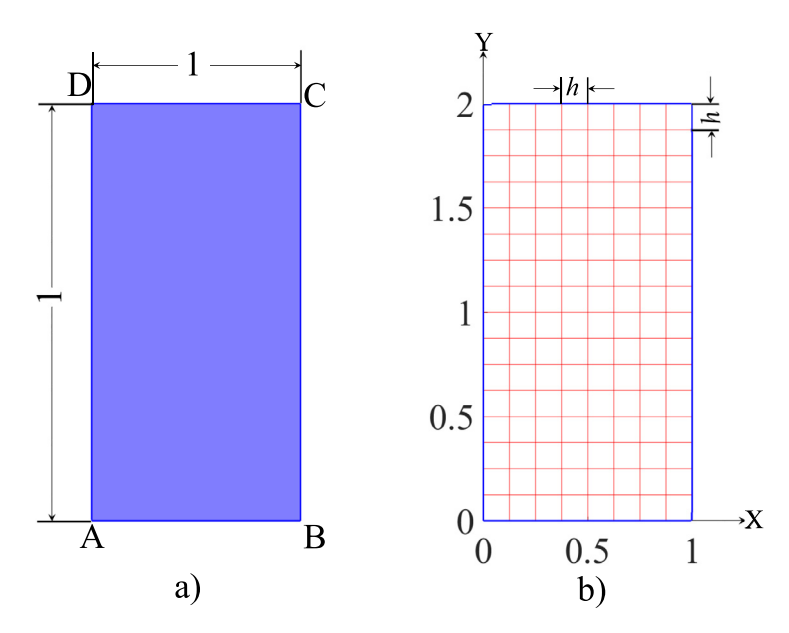


Fig. 3. A rectangular plate (a) as well as an example of a structured square  $(b_y = 1)$  mesh (b) used by the new approach and by the conventional finite elements.

#### 3.1. 2-D wave propagation in isotropic and anisotropic inhomogeneous materials

In this section two test problems for the 2-D wave equation with variable coefficients for isotropic and anisotropic inhomogeneous materials (Eq. (1)) are solved by the new approach and by the conventional finite elements. The method of manufactured solutions (e.g., see [70]) is used to construct the exact solutions for the test problems considered below. The following exact solutions are used:

$$u(x, y, t) = \sin[5\pi(x+y)]\cos(3\pi t)$$
(23)

with  $c_x^2 = c_y^2 = 6 + 4sin(3xy)$  for the isotropic material and

$$u(x, y, t) = \cos(5\pi x)\sin(4\pi y)\cos(2\pi t) \tag{24}$$

with  $c_x^2 = 8 + 5\cos(3x + 2y)$  and  $c_y^2 = 6 + 4\sin(3xy)$  for the anisotropic material.

#### 3.1.1. A rectangular plate

First, we solve the test problems for the rectangular plate ABCD by the new approach and by the conventional finite elements on structured square  $(b_y = 1)$  meshes; see Fig. 3. Fig. 4 shows the maximum relative errors in displacement  $e_u^{max}$  and in velocity  $e_v^{max}$  as a function of the mesh size h in the logarithmic scale. It can be seen from Fig. 4 that the order of accuracy for the new approach is close to 4 (the slope of the curves in Fig. 4 at small h represents the order of accuracy). It is also apparent from Fig. 4 that at the same h the new approach yields much more accurate results than those obtained by the conventional linear and quadratic finite elements.

**Remark 6.** The mesh size h for the high-order finite elements on uniform meshes is defined as the distance between two consecutive nodes along x-axis. Therefore, at the same h the high-order finite elements have exactly same number of degrees of freedom as the linear finite elements and the new approach.

#### 3.1.2. A complex irregular domain

Here, the same test problems are solved by the new approach as well as by the conventional finite elements for the trapezoidal plate with two holes (see Fig. 5a). Fig. 6 shows the distribution of the exact solutions for the displacement and the velocity as well as the distribution of the relative errors in displacement and in velocity of

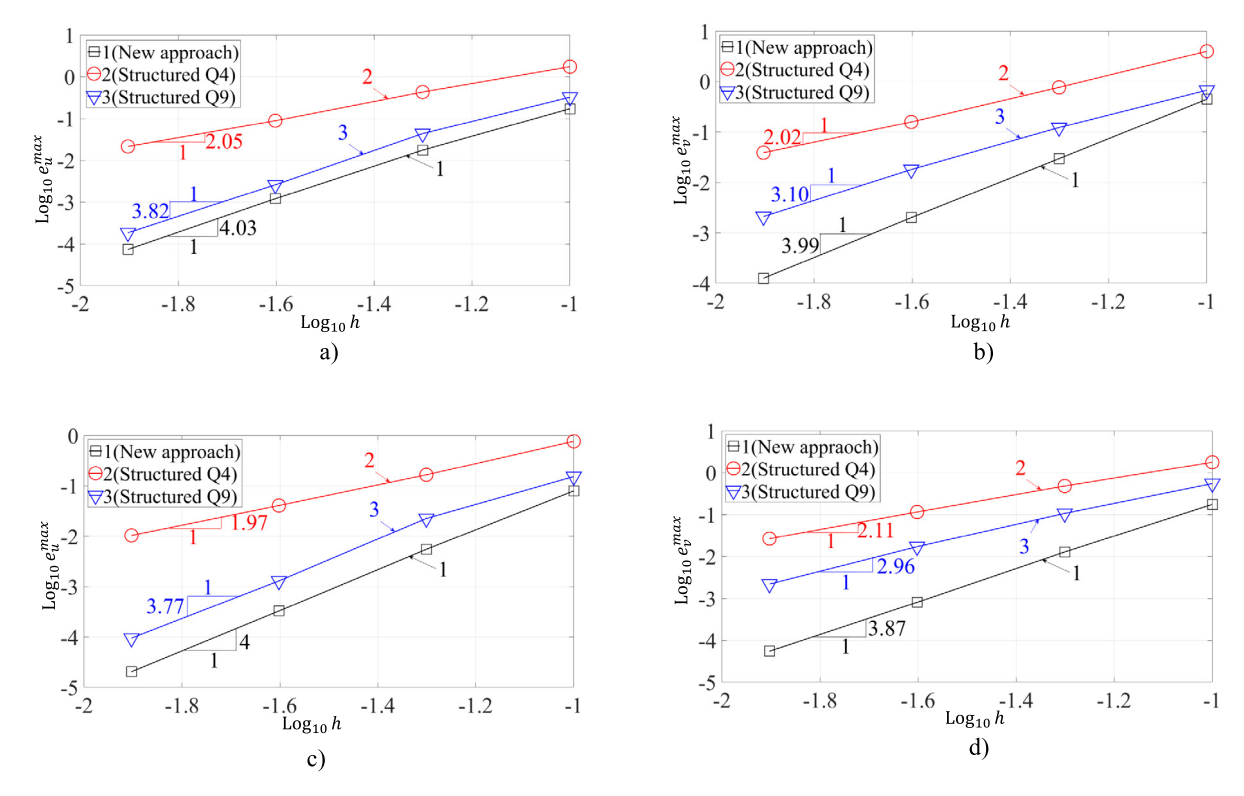


Fig. 4. The maximum relative errors in displacement  $e_u^{max}$  (a, c) and in velocity  $e_v^{max}$  (b, d) at the final time T=0.2 for the rectangular plate (see Fig. 3) as a function of the mesh size h in the logarithmic scale. The numerical solutions of the 2-D wave equation for the isotropic (a, b) and anisotropic (c, d) inhomogeneous materials are obtained by the new approach (curve 1) and by the conventional linear and quadratic finite elements (curves 2 and 3) on structured square ( $h_y=1$ ) meshes. Symbols  $\square$ ,  $\square$  and  $\triangledown$  correspond to the results for the different h used in calculations.

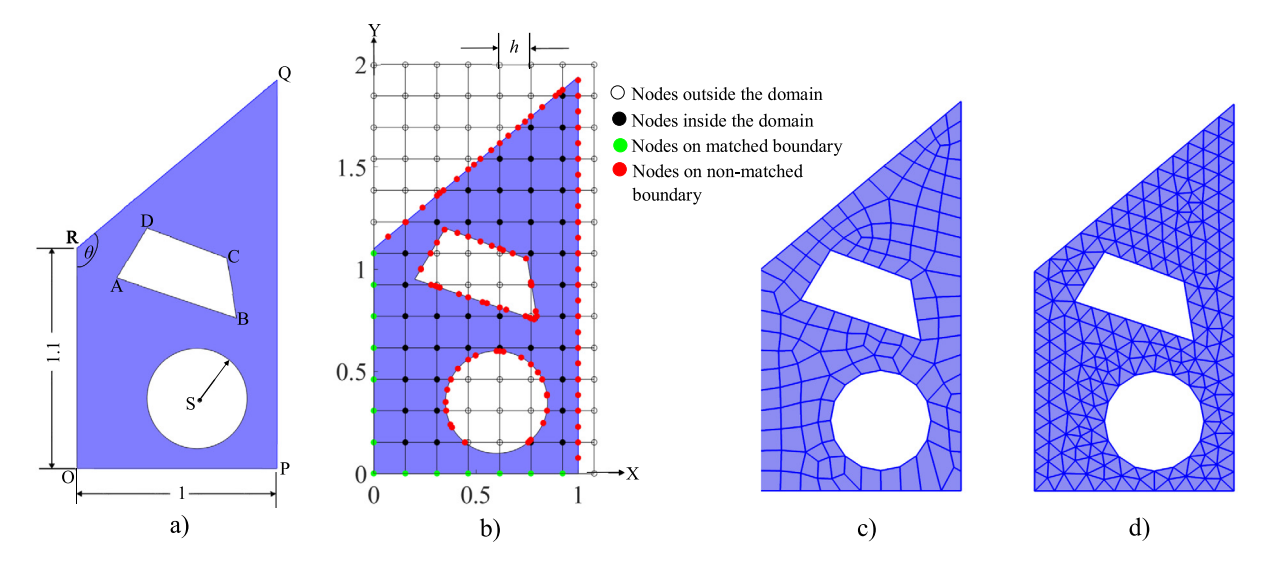


Fig. 5. A trapezoidal plate OPQR ( $\theta = 130^{\circ}$ ) with a circular hole of radius 0.25 centered at S(0.6, 0.35) and a quadrilateral hole ABCD (A(0.2, 0.95), B(0.8, 0.75), C(0.75, 1.05), D(0.35, 1.2)) (a) as well as a Cartesian mesh for the new approach (b). Examples of typical quadrilateral (c) and triangular (d) finite element meshes generated by the commercial software COMSOL for the discretization of the plate OPQR.

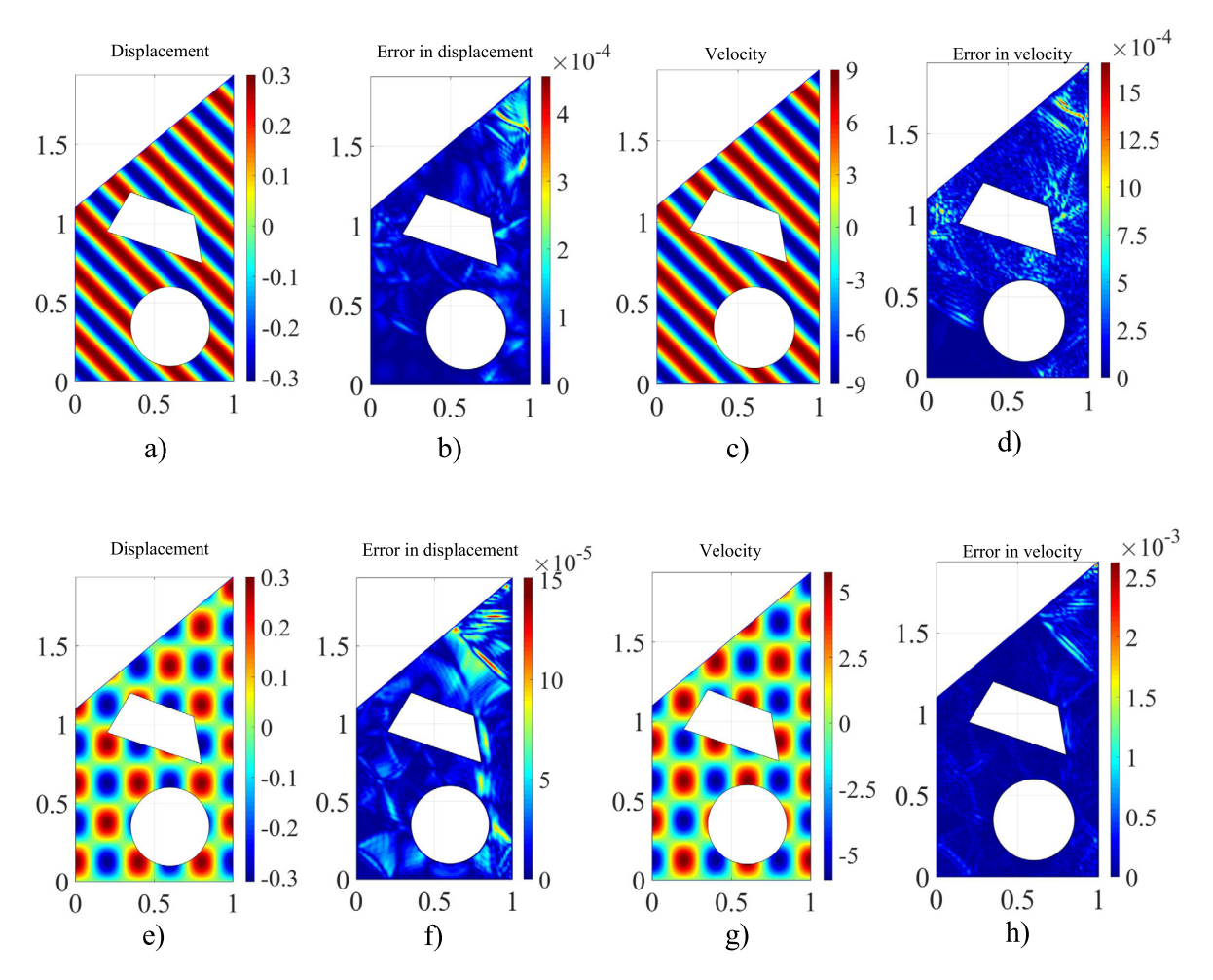


Fig. 6. The distribution of the exact solutions for the displacement u(x, y) (a, e) and the velocity v(x, y) (c, g) as well as the relative errors in displacement  $e_u(x, y)$  (b, f) and in velocity  $e_v(x, y)$  (d, h) of the numerical solutions at the final time T = 0.2. The isotropic (a-d) and anisotropic (e-h) inhomogeneous materials are considered. The numerical solutions of the 2-D wave equation are obtained by the new approach on the square  $(b_v = 1)$  Cartesian mesh of size h = 1/80.

the numerical solution obtained by the new approach on the square Cartesian mesh of size h = 1/80. As can be seen from Fig. 6b, d, f, h the numerical results obtained by the new approach on this mesh are very accurate (the errors are small).

In order to compare the accuracy of the numerical results obtained by the new approach and by finite elements, Fig. 7 illustrates the errors  $e_u^{max}$  and  $e_v^{max}$  of the numerical techniques as a function of the number of degrees of freedom N in the logarithmic scale. It can be seen from Fig. 7 that at the same number of degrees of freedom the results obtained by the new approach are more accurate than those obtained by the conventional linear and high-order (up to third order) finite elements; see the curves at the same N. We should mention that this increase in accuracy is impressive considering the fact that the width of the stencils and the computational costs for the high-order finite elements are much greater compared to those for the new approach (the width of the stencils for the new approach is same as that for the linear quadrilateral finite elements). This improvement in accuracy also means that at a given accuracy the new approach requires much less number of degrees of freedom compared to that for the conventional (up to third order) finite elements.

For the new approach on irregular domains, the mesh size h is approximately proportional to  $1/\sqrt{N}$  (this statement is strictly valid for a rectangular plate with matched Cartesian meshes). Therefore, the slope of curves 1 in Fig. 7 at large  $\sqrt{N}$  approximately describes the order of accuracy of the new approach. As can be seen from

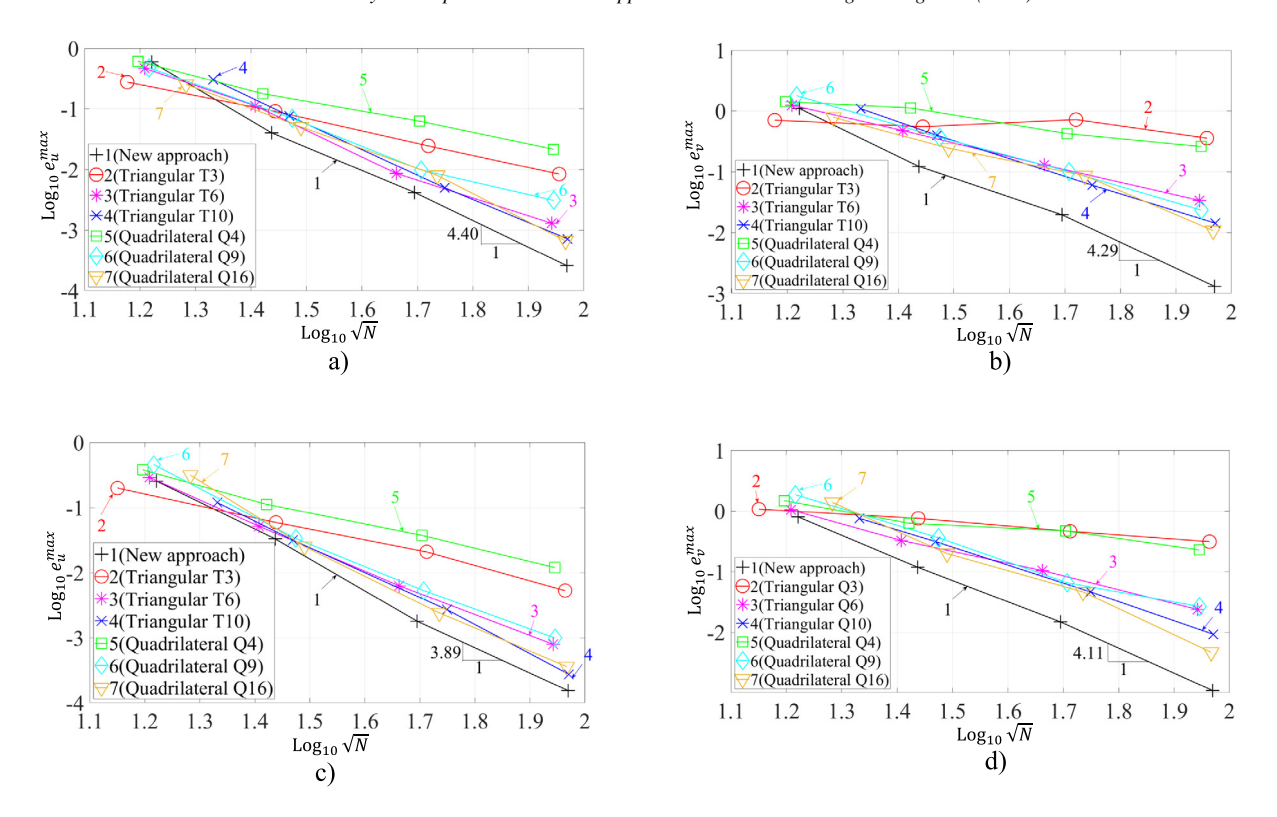


Fig. 7. The maximum relative errors in displacement  $e_u^{max}$  (a, c) and in velocity  $e_v^{max}$  (b, d) at the final time T=0.2 for the trapezoidal plate (see Fig. 5a) as a function of  $\sqrt{N}$  in the logarithmic scale; N is the number of degrees of freedom. The numerical solutions of the 2-D wave equation for the isotropic (a, b) and anisotropic (c, d) inhomogeneous materials are obtained by the new approach on square  $(b_y = 1)$  Cartesian meshes (curve 1) and by the conventional triangular (curves 2-4) and quadrilateral (curves 5-7) finite elements. Curves (2, 5), (3, 6) and (4, 7) correspond to the linear, quadratic and cubic finite elements, respectively. Symbols +,  $\bigcirc$ , \*,  $\times$ ,  $\square$ ,  $\diamond$  and  $\triangledown$  correspond to the results for the different N used in calculations.

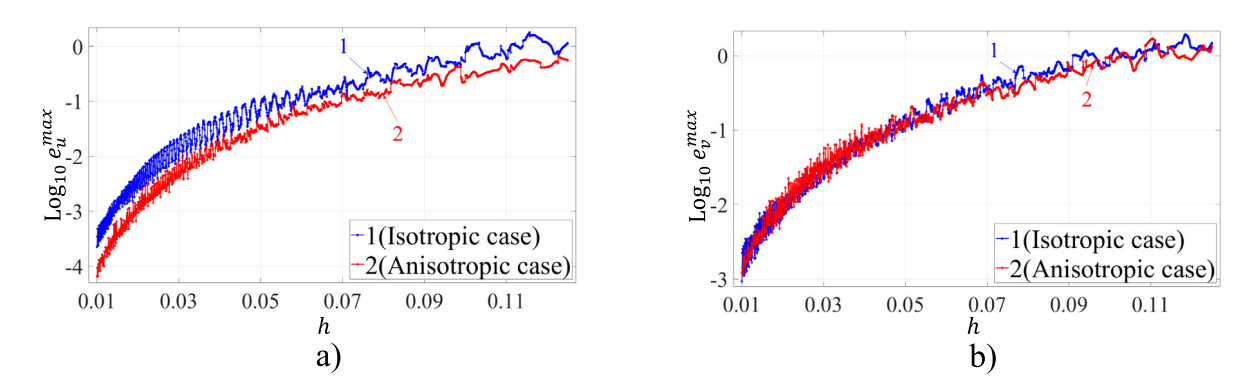
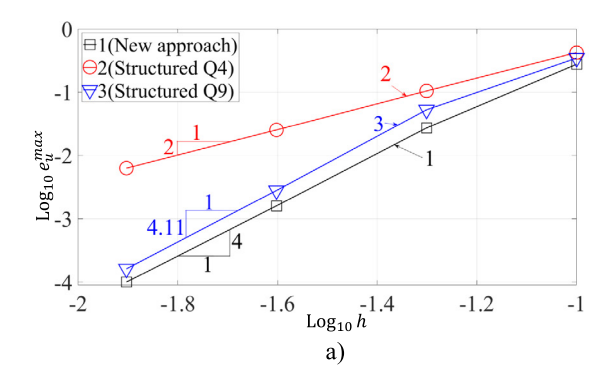


Fig. 8. The maximum relative errors in displacement  $e_u^{max}$  (a) and in velocity  $e_v^{max}$  (b) at the final time T=0.2 for the trapezoidal plate (see Fig. 5a) as a function of the mesh size h in the logarithmic scale. The numerical solutions of the 2-D wave equation for the isotropic (curve 1) and anisotropic (curve 2) inhomogeneous materials are obtained by the new approach on 1500 square ( $b_y=1$ ) Cartesian meshes.

Fig. 7, the order of accuracy of the new approach for the wave equation with variable coefficients is close to four for isotropic and the anisotropic materials. This is in agreement with the theoretical results in Section 2.

In order to study the convergence of the numerical results obtained by the new approach in more detail, Fig. 8 presents curves 1 in Fig. 7 at small changes of the mesh size h (curves 1 and 2 in Fig. 8a correspond to curves



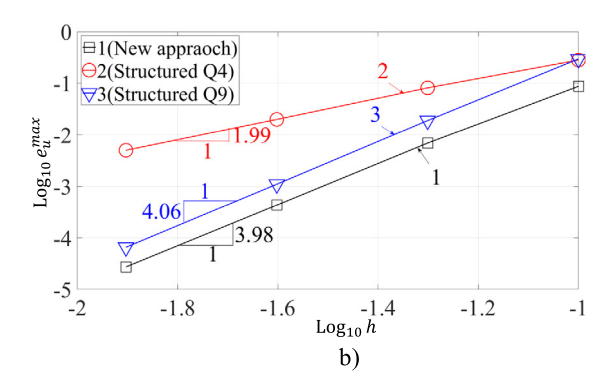


Fig. 9. The maximum relative error in temperature  $e_u^{max}$  at the final time T=0.2 for the rectangular plate (see Fig. 3) as a function of the mesh size h in the logarithmic scale. The numerical solutions of the 2-D heat equation for the isotropic (a) and anisotropic (b) inhomogeneous materials are obtained by the new approach (curve 1) and by the conventional linear and quadratic finite elements (curves 2 and 3) on structured square ( $b_v = 1$ ) meshes. Symbols  $\Box$ ,  $\bigcirc$  and  $\bigtriangledown$  correspond to the results for the different h used in calculations.

1 in Fig. 7a and c; curves 1 and 2 in Fig. 8b correspond to curves 1 in Fig. 7b and d). For this study, we solve the test problems on 1500 Cartesian meshes with the mesh sizes  $h_i = h_1 + \frac{(h_2 - h_1)(i-1)}{1499}$  where  $h_1 = 1/8 = 0.125$ ,  $h_2 = 1/100 = 0.01$  and  $i = 1, 2, 3, \ldots, 1500$ . As can be seen from Fig. 8 the new approach yields convergent and stable results with small oscillations. This oscillatory behavior can be explained by (a) the complicated dependency of the leading terms of the local truncation error on the coefficients  $d_i$  and (b) at small variations of the mesh size h, there is a discontinuous change in the location of the grid points with respect to the irregular boundary (e.g., some grid points that are the internal points for the previous mesh can move to the boundary or outside the boundary for the next mesh); this leads to the discontinuous change of some stencils equations for the meshes with the small difference in h. It is important to mention that small oscillations in the numerical convergence curves are typical for many numerical techniques on irregular domains at small variations of h. For example, the change in the angles of the finite elements at small variations of the element size h also leads to such oscillations in the convergence curves for the finite element techniques.

It can be concluded that at the same number of degrees of freedom, the new numerical approach for the 2-D wave equation with variable coefficients for isotropic and anisotropic materials yields much more accurate results compared to those obtained by the linear and high-order (quadratic and cubic) finite elements. It is worth to mention that the high-order finite elements have much wider stencils and require greater computational time compared to those for the new approach.

#### 3.2. 2-D heat transfer in isotropic and anisotropic inhomogeneous materials

In this section two test problems for the 2-D heat equation with variable coefficients for isotropic and anisotropic inhomogeneous materials (Eq. (2)) are solved by the new approach and by the conventional finite elements. The following exact solutions are used for the test problems:

$$u(x, y, t) = 100sin(5\pi x)cos(10\pi y)e^{-2\pi t}$$
(25)

with  $a_x = a_y = 7 + 3e^{xy}$  for the isotropic material and

$$u(x, y, t) = 500\cos[\pi(7x + 5y)]e^{-3\pi t}$$
(26)

with  $a_x = 7 + 3e^{xy}$  and  $a_y = 4 + 0.5e^{2x+y-1}$  for the anisotropic material.

#### 3.2.1. A rectangular plate

Similar to Section 3.1.1, first we solve the test problems for the rectangular plate ABCD by the new approach and by the conventional finite elements on structured square  $(b_y = 1)$  meshes; see Fig. 3. Fig. 9 shows the maximum relative error in temperature  $e_u^{max}$  as a function of the mesh size h in the logarithmic scale. As can be seen from Fig. 9 the order of accuracy of the new approach is close to four (the slope of the curves in Fig. 9 at small h represents

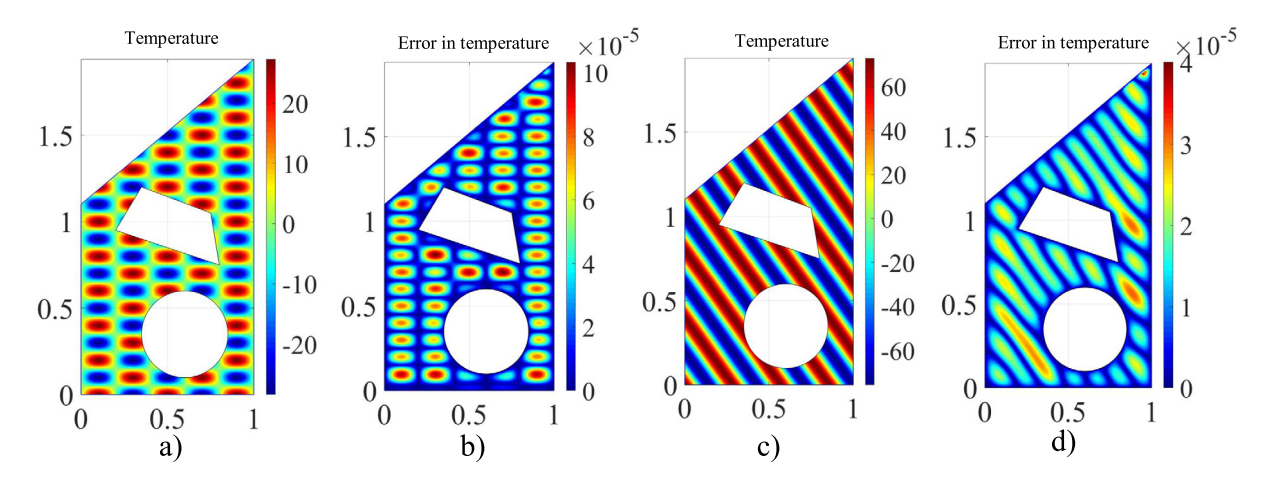


Fig. 10. The distribution of the exact solutions for the temperature u(x, y) (a, c) as well as the relative error in temperature  $e_u(x, y)$  (b, d) of the numerical solution at the final time T = 0.2. The isotropic (a, b) and anisotropic (c, d) inhomogeneous materials are considered. The numerical solutions of the 2-D heat equation are obtained by the new approach on the square  $(b_y = 1)$  Cartesian mesh of size h = 1/80.

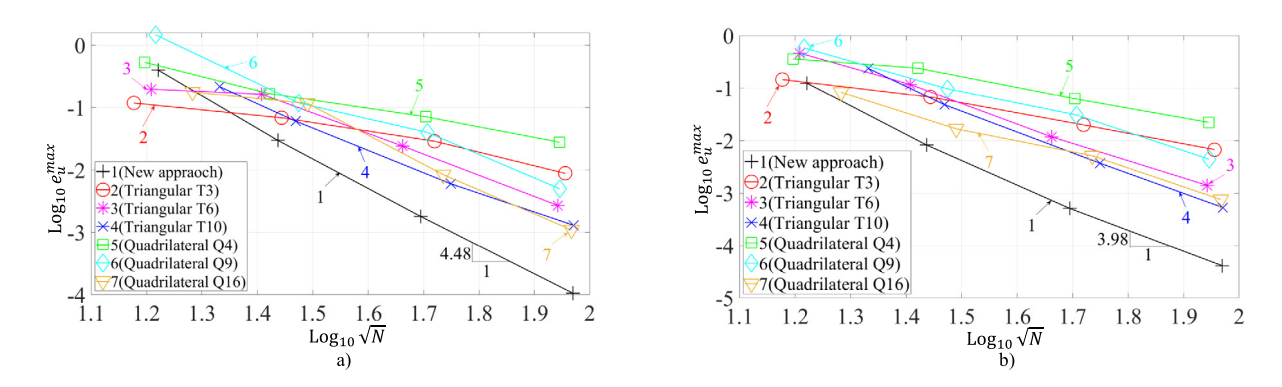


Fig. 11. The maximum relative errors in temperature  $e_u^{max}$  at the final time T=0.2 for the trapezoidal plate (see Fig. 5a) as a function of  $\sqrt{N}$  in the logarithmic scale; N is the number of degrees of freedom. The numerical solutions of the 2-D heat equation for the isotropic (a) and anisotropic (b) inhomogeneous materials are obtained by the new approach on square  $(b_y=1)$  Cartesian meshes (curve 1) and by the conventional triangular (curves 2-4) and quadrilateral (curves 5-7) finite elements. Curves (2, 5), (3, 6) and (4, 7) correspond to the linear, quadratic and cubic finite elements, respectively. Symbols +,  $\bigcirc$ , \*,  $\times$ ,  $\square$ ,  $\diamond$  and  $\triangledown$  correspond to the results for the different N used in calculations.

the order of accuracy). It is also demonstrated in Fig. 9 that the new approach yields much more accurate results than those obtained by the linear and quadratic finite elements at the same mesh size h.

#### 3.2.2. A complex irregular domain

Here, the same test problems are solved by the new approach as well as by the conventional finite elements for the trapezoidal plate (see Fig. 5a). Fig. 10 shows the distribution of the exact solutions for the temperature as well as the distribution of the relative error in temperature of the numerical solution obtained by the new approach on the square Cartesian mesh of size h = 1/80. As can be seen from Fig. 10 the numerical results obtained by the new approach on this mesh are very accurate (the errors are small).

In order to compare the accuracy of the numerical results obtained by the new approach and by finite elements, Fig. 11 illustrates the errors  $e_u^{max}$  of the numerical techniques as a function of the number of degrees of freedom N in the logarithmic scale. It can be seen from Fig. 11 that at the same number N of degrees of freedom, the results obtained by the new approach are more accurate than those obtained by the conventional linear and high-order (quadratic and cubic) finite elements. This increase in accuracy is impressive considering the fact that the width of the stencils and the computational costs for the high-order finite elements are much greater compared to those

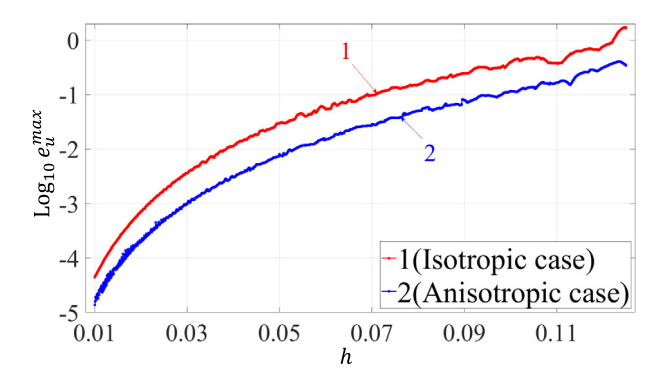


Fig. 12. The maximum relative errors in temperature  $e_u^{max}$  at the final time T=0.2 for the trapezoidal plate (see Fig. 5a) as a function of the mesh size h in the logarithmic scale. The numerical solutions of the 2-D heat equation for the isotropic (curve 1) and anisotropic (curve 2) inhomogeneous materials are obtained by the new approach on 1500 square ( $b_v = 1$ ) Cartesian meshes.

for the new approach. Similar to Fig. 7 for the 2-D wave equation, it can be seen from Fig. 11 that the order of accuracy of the new approach on the complex irregular domains is close to four for the 2-D heat equation with variable coefficients as well; see the slope of curves 1 in Fig. 11 at large N. This is in agreement with the theoretical results in Section 2.

In order to study the convergence of the numerical solutions obtained by the new approach in more detail, we solve the same test problems on 1500 Cartesian meshes with small variations of the grid size h and show the convergence curves in Fig. 12 (see Section 3.1.2 for the selection of h). As can be seen, the new approach yields convergent and stable numerical results for the heat equation with variable coefficients.

It can be concluded that at the same number of degrees of freedom, the new approach for the 2-D heat equation with variable coefficients for isotropic and anisotropic materials yields much more accurate results compared to those obtained by the linear and high-order (quadratic and cubic) finite elements. We should mention that the high-order finite elements have much wider stencils and require greater computational time compared to those for the new approach.

#### 4. Concluding remarks

The new numerical approach developed in this paper is the extension of our approach for the wave and heat equations with constant coefficients (see [61–63]) to a much more general case of variable coefficients. The main idea that allows this extension is the representation of the stencil coefficients  $\bar{m}_i(h)$  and  $\bar{k}_i(h)$  as polynomial functions of the mesh size h. Despite the use of 63 unknown coefficients  $m_{i,p}$ ,  $k_{j,p}(i=0,1,j=0,1,2,3,4,p=1,2,\ldots,9)$  for each 9-point stencil, they are combined into 18 stencil coefficients  $\bar{m}_i(h)$  and  $\bar{k}_i(h)$  ( $i=1,2,\ldots,9$ ) that are used in the global matrix; i.e., the size of the global semidiscrete system is the same for the wave (heat) equation with constant and variable coefficients. The increase in the computational costs for the calculation of 63 unknown coefficients from the local system of equations is insignificant compared to the computational costs for the integration of the global semidiscrete equations. The numerical approach developed here for the wave (heat) equation with variable coefficients provides the same fourth order of accuracy as that developed in [61–63] for the wave (heat) equation with constant coefficients.

The main advantages of the suggested technique can be summarized as follows:

• Many difficulties of the existing numerical techniques for irregular domains (e.g., the finite elements, spectral element, isogeometric elements, the finite volume method, and many other) are related to complicated mesh generators and the accuracy of 'bad' elements (e.g., the elements with small angles). In contrast to these techniques, the new approach is based on trivial Cartesian meshes with a trivial procedure for the formation of the 9-point nonuniform stencils for the grid points located close to the boundary. Moreover, very small distances between the grid points of a Cartesian mesh and the boundary (i.e., when some coefficients  $d_i$  of the non-uniform stencil are close to zero while some other coefficients  $d_i$  of the same stencil equal unity; see Fig. 2) does not decrease the accuracy of the new technique.

- In contrast to the finite-difference techniques with the stencil coefficients calculated through the approximation of separate partial derivatives, the entire partial differential equation is used for the calculation of the stencil coefficients in the new approach. This leads to the optimal accuracy of the proposed technique. E.g., the 9-point uniform and nonuniform stencils of the new approach provide the optimal accuracy that cannot be improved without changing the width of stencil equations. In contrast to the 9-point stencils of the linear quadrilateral finite elements, the new approach yields a much higher order of accuracy (the increase by two orders).
- The numerical results for irregular domains also show that at the same number of degrees of freedom, the new approach is even much more accurate than the high-order (up to the third order) finite elements with much wider stencils. This also means that at a given accuracy, the new approach significantly reduces the computation time compared to that for the linear and high-order finite elements.
- The new approach does not require time consuming numerical integration for finding the coefficients of the stencil equations; e.g., as for the high-order finite, spectral and isogeometric elements. For the new technique, the coefficients of the uniform stencils for the grid points located far from the boundary are calculated analytically. For the grid points located close to the boundary, the coefficients of the nonuniform stencils are calculated numerically by the solution of small local systems of linear algebraic equations. Numerical experiments show that the solution of these small local systems of algebraic equations is fast. Moreover, these local systems are independent of each other and can be efficiently solved on a parallel computer.
- It has been shown that the wave and heat equations can be uniformly treated with the new approach. The order of the time derivative in these equations does not affect the coefficients of the stencil equations of the semi-discrete systems because in the presented derivations the space discretization is considered independent of the time discretization without the interaction between the errors in space and time.

It is interesting to note that the final formulas for the calculation of the stencil coefficients do not include the derivatives of the solution and the new approach can be also applied to the problems with reduced regularity (smoothness). In our paper [62] the 1-D impact wave propagation problem with a propagating discontinuity has been solved by the new approach on matched and non-matched meshes as well as by the conventional finite elements. The numerical results in [62] show that even in this case the new approach yields more accurate results compared to those obtained by the conventional finite elements. We observed similar effects for the isogeometric elements applied to the same 1-D impact problem; i.e., the approximation of discontinuous solutions by smooth functions of high-order isogeometric elements yields accurate results.

In the future we plan to consider the stencils with a larger number of grid points for a higher order of accuracy (similar to the high-order finite elements or to the high-order finite-difference techniques), to consider a mesh refinement with uniform Cartesian meshes using special stencils for the transition from a fine mesh to a coarse mesh, to apply the proposed technique to other PDEs with variable coefficients.

### **Declaration of competing interest**

The authors declare that they have no known competing financial interests or personal relationships that could have appeared to influence the work reported in this paper.

#### Acknowledgments

The research has been supported in part by the NSF, USA grant CMMI-1935452 and by Texas Tech University, USA.

Appendix A. The detailed expression for the local truncation error e in Eq. (14) and the coefficients  $b_p$  used in Eq. (14)

$$e = \bar{c}\{b_{1}u_{5} + h[b_{2}\frac{\partial u_{5}}{\partial x} + b_{3}\frac{\partial u_{5}}{\partial y} + b_{4}u_{5}] + h^{2}[b_{5}\frac{\partial^{2}u_{5}}{\partial x^{2}} + b_{6}\frac{\partial^{2}u_{5}}{\partial x\partial y} + b_{7}\frac{\partial u_{5}}{\partial x} + b_{8}\frac{\partial^{2}u_{5}}{\partial y^{2}} + b_{9}\frac{\partial u_{5}}{\partial y} + b_{10}u_{5}]$$

$$+h^{3}[b_{11}\frac{\partial^{3}u_{5}}{\partial x^{3}} + b_{12}\frac{\partial^{3}u_{5}}{\partial x^{2}\partial y} + b_{13}\frac{\partial^{2}u_{5}}{\partial x^{2}} + b_{14}\frac{\partial^{3}u_{5}}{\partial x\partial y^{2}} + b_{15}\frac{\partial^{2}u_{5}}{\partial x\partial y} + b_{16}\frac{\partial u_{5}}{\partial x} + b_{17}\frac{\partial^{3}u_{5}}{\partial y^{3}} + b_{18}\frac{\partial^{2}u_{5}}{\partial y^{2}}$$

$$+b_{19}\frac{\partial u_{5}}{\partial y} + b_{20}u_{5}]$$

$$+ h^{4}[b_{21}\frac{\partial^{4}u_{5}}{\partial x^{4}} + b_{22}\frac{\partial^{4}u_{5}}{\partial x^{3}\partial y} + b_{23}\frac{\partial^{3}u_{5}}{\partial x^{3}} + b_{24}\frac{\partial^{4}u_{5}}{\partial x^{2}\partial y^{2}} + b_{25}\frac{\partial^{3}u_{5}}{\partial x^{2}\partial y} + b_{26}\frac{\partial^{2}u_{5}}{\partial x^{2}} + b_{27}\frac{\partial^{4}u_{5}}{\partial x\partial y^{3}} + b_{28}\frac{\partial^{3}u_{5}}{\partial x^{2}\partial y} + b_{29}\frac{\partial^{2}u_{5}}{\partial x\partial y} + b_{30}\frac{\partial u_{5}}{\partial x} + b_{31}\frac{\partial^{4}u_{5}}{\partial y^{4}} + b_{32}\frac{\partial^{3}u_{5}}{\partial y^{3}} + b_{33}\frac{\partial^{2}u_{5}}{\partial y^{2}} + b_{34}\frac{\partial u_{5}}{\partial y} + b_{35}u_{5}]$$

$$+ h^{5}[b_{36}\frac{\partial^{5}u_{5}}{\partial x^{5}} + b_{37}\frac{\partial^{5}u_{5}}{\partial x^{4}\partial y} + b_{38}\frac{\partial^{4}u_{5}}{\partial x^{4}} + b_{39}\frac{\partial^{5}u_{5}}{\partial x^{3}\partial y^{2}} + b_{40}\frac{\partial^{4}u_{5}}{\partial x^{3}\partial y} + b_{41}\frac{\partial^{3}u_{5}}{\partial x^{3}} + b_{42}\frac{\partial^{5}u_{5}}{\partial x^{2}\partial y^{3}} + b_{43}\frac{\partial^{5}u_{5}}{\partial x^{2}\partial y^{3}} + b_{44}\frac{\partial^{3}u_{5}}{\partial x^{2}\partial y} + b_{45}\frac{\partial^{2}u_{5}}{\partial x^{2}} + b_{46}\frac{\partial^{5}u_{5}}{\partial x\partial y^{4}} + b_{47}\frac{\partial^{4}u_{5}}{\partial x\partial y^{3}} + b_{48}\frac{\partial^{3}u_{5}}{\partial x\partial y^{2}} + b_{49}\frac{\partial^{2}u_{5}}{\partial x\partial y} + b_{50}\frac{\partial^{2}u_{5}}{\partial x} + b_{50}\frac{\partial^{2}u_{5}}{\partial x} + b_{50}\frac{\partial^{2}u_{5}}{\partial y} + b_{50}\frac{\partial^{2}u_{5}}{\partial x} + b_{50}\frac{\partial^{2}u_{5}}{$$

The first ten coefficients  $b_i$  ( $i=1,2,\ldots,10$ ) are presented below. All coefficients  $b_i$  ( $i=1,2,\ldots,165$ ) used in the paper are given in Appendix D.

$$\begin{aligned} b_1 &= k_{0,1} + k_{0,2} + k_{0,3} + k_{0,4} + k_{0,5} + k_{0,6} + k_{0,7} + k_{0,8} + k_{0,9} \\ b_2 &= -d_1k_{0,1} + d_3k_{0,3} - d_4k_{0,4} + d_5k_{0,6} - d_6k_{0,7} + d_8k_{0,9} \\ b_3 &= -d_1k_{0,1} - d_2k_{0,2} - d_3k_{0,3} + d_6k_{0,7} + d_7k_{0,8} + d_8k_{0,9} \\ b_4 &= k_{1,1} + k_{1,2} + k_{1,3} + k_{1,4} + k_{1,5} + k_{1,6} + k_{1,7} + k_{1,8} + k_{1,9} \\ b_5 &= \frac{1}{2}(2\bar{c}_x(x,y)(m_{0,1} + m_{0,2} + m_{0,3} + m_{0,4} + m_{0,5} + m_{0,6} + m_{0,7} + m_{0,8} + m_{0,9}) + d_1^2k_{0,1} \\ &+ d_3^2k_{0,3} + d_4^2k_{0,4} + d_5^2k_{0,6} + d_6^2k_{0,7} + d_8^2k_{0,9}) \\ b_6 &= d_1^2k_{0,1} - d_3^2k_{0,3} - d_6^2k_{0,7} + d_8^2k_{0,9} \\ b_7 &= \bar{c}_x^{(1,0)}(x,y)(m_{0,1} + m_{0,2} + m_{0,3} + m_{0,4} + m_{0,5} + m_{0,6} + m_{0,7} + m_{0,8} + m_{0,9}) - d_1k_{1,1} \\ &+ d_3k_{1,3} - d_4k_{1,4} + d_5k_{1,6} - d_6k_{1,7} + d_8k_{1,9} \\ b_8 &= \frac{1}{2}(2\bar{c}_y(x,y)(m_{0,1} + m_{0,2} + m_{0,3} + m_{0,4} + m_{0,5} + m_{0,6} + m_{0,7} + m_{0,8} + m_{0,9}) + d_1^2k_{0,1} \\ &+ d_2^2k_{0,2} + d_3^2k_{0,3} + d_6^2k_{0,7} + d_7^2k_{0,8} + d_8^2k_{0,9}) \\ b_9 &= \bar{c}_y^{(0,1)}(x,y)(m_{0,1} + m_{0,2} + m_{0,3} + m_{0,4} + m_{0,5} + m_{0,6} + m_{0,7} + m_{0,8} + m_{0,9}) - d_1k_{1,1} \\ &- d_2k_{1,2} - d_3k_{1,3} + d_6k_{1,7} + d_7k_{1,8} + d_8k_{1,9} \\ b_{10} &= k_{2,1} + k_{2,2} + k_{2,3} + k_{2,4} + k_{2,5} + k_{2,6} + k_{2,7} + k_{2,8} + k_{2,9} \end{aligned}$$

# Appendix B. The coefficients $m_{i,p}$ , $k_{j,p}$ ( $i=0,1,j=0,1,2,3,4,p=1,2,\ldots,9$ ) for the 9-point uniform stencil and the corresponding local truncation error

$$m_{0,1} = \frac{1}{240(\bar{c}_x(x,y) + \bar{c}_y(x,y))}, \quad m_{1,2} = \frac{1}{24(\bar{c}_x(x,y) + \bar{c}_y(x,y))}, \quad m_{0,3} = \frac{1}{240(\bar{c}_x(x,y) + \bar{c}_y(x,y))}, \quad m_{0,4} = \frac{1}{24(\bar{c}_x(x,y) + \bar{c}_y(x,y))}, \quad m_{0,6} = \frac{1}{24(\bar{c}_x(x,y) + \bar{c}_y(x,y))}, \quad m_{0,6} = \frac{1}{24(\bar{c}_x(x,y) + \bar{c}_y(x,y))}, \quad m_{0,7} = \frac{1}{240(\bar{c}_x(x,y) + \bar{c}_y(x,y))}, \quad m_{0,8} = \frac{1}{24(\bar{c}_x(x,y) + \bar{c}_y(x,y))}, \quad m_{0,8} = \frac{1}{24(\bar{c}_x(x,y) + \bar{c}_y(x,y))}, \quad m_{0,9} = \frac{1}{240(\bar{c}_x(x,y) + \bar{c}_y(x,y))}, \quad m_{1,1} = \frac{\bar{c}_x(x,y)\bar{c}_y^{(0,1)}(x,y) + \bar{c}_y(x,y)\bar{c}_x^{(1,0)}(x,y)}{480\bar{c}_x(x,y)\bar{c}_y^{(1,0)}(x,y) + \bar{c}_y(x,y)\bar{c}_x^{(1,0)}(x,y)}, \quad m_{1,2} = \frac{\bar{c}_y^{(0,1)}(x,y)}{48\bar{c}_y(x,y)\bar{c}_y^{(1,0)}(x,y) + \bar{c}_y(x,y)}, \quad m_{1,8} = -\frac{\bar{c}_x^{(1,0)}(x,y)}{48\bar{c}_y(x,y)\bar{c}_x^{(1,0)}(x,y)}, \quad m_{1,9} = -\frac{\bar{c}_x(x,y)\bar{c}_y^{(0,1)}(x,y) + \bar{c}_y(x,y)}{480\bar{c}_x(x,y)\bar{c}_y(x,y) + \bar{c}_y(x,y)}, \quad m_{1,9} = -\frac{\bar{c}_x(x,y)\bar{c}_y^{(0,1)}(x,y) + \bar{c}_y(x,y)}{480\bar{c}_x(x,y)\bar{c}_y(x,y) + \bar{c}_y(x,y)}, \quad m_{1,9} = -\frac{\bar{c}_x(x,y)\bar{c}_y^{(0,1)}(x,y) + \bar{c}_y(x,y)}{480\bar{c}_x(x,y)\bar{c}_y(x,y) + \bar{c}_y(x,y)}, \quad m_{1,9} = -\frac{\bar{c}_x(x,y)\bar{c}_y^{(0,1)}(x,y) + \bar{c}_y(x,y)\bar{c}_x(x,y) + \bar{c}_y(x,y)}{480\bar{c}_x(x,y)\bar{c}_y(x,y) + \bar{c}_y(x,y)}, \quad m_{1,9} = -\frac{\bar{c}_x(x,y)\bar{c}_y^{(0,1)}(x,y) + \bar{c}_y(x,y)\bar{c}_x(x,y) + \bar{c}_y(x,y)}{480\bar{c}_x(x,y)\bar{c}_x(x,y) + \bar{c}_y(x,y)}, \quad m_{1,9} = -\frac{\bar{c}_x(x,y)\bar{c}_y^{(0,1)}(x,y) + \bar{c}_y(x,y)\bar{c}_x(x,y) + \bar{c}_y(x,y)}{480\bar{c}_x(x,y)\bar{c}_y(x,y)\bar{c}_x(x,y) + \bar{c}_y(x,y)}, \quad m_{1,9} = -\frac{\bar{c}_x(x,y)\bar{c}_y^{(0,1)}(x,y) + \bar{c}_y(x,y)\bar{c}_x(x,y) + \bar{c}_y(x,y)}{480\bar{c}_x(x,y)\bar{c}_y(x,y)\bar{c}_x(x,y) + \bar{c}_y(x,y)}, \quad m_{1,9} = -\frac{\bar{c}_x(x,y)\bar{c}_y^{(0,1)}(x,y) + \bar{c}_y(x,y)\bar{c}_x(x,y) + \bar{c}_y(x,y)}{480\bar{c}_x(x,y)\bar{c}_x(x,y) + \bar{c}_y(x,y)}, \quad m_{1,9} = -\frac{\bar{c}_x(x,y)\bar{c}_y^{(0,1)}(x,y) + \bar{c}_y(x,y)\bar{c}_x(x,y) + \bar{c}_y(x,y)}{480\bar{c}_x(x,y)\bar{c}_x(x,y) + \bar{c}_y(x,y)}, \quad m_{1,9} = -\frac{\bar{c}_x(x,y)\bar{c}_y^{(0,1)}(x,y) + \bar{c}_y(x,y)\bar{c}_x(x,y) + \bar{c}_y(x,y)}{480\bar{c}_x(x,y)\bar{c}_x(x,y) + \bar{c}_y(x,y)}, \quad m_{1,9} = -\frac{\bar{c}_x$$

```
\bar{c}_x(x, y) - 5\bar{c}_y(x, y)
  k_{0,1} = -\frac{1}{20}, \qquad k_{0,2} = \frac{c_x(x, y) - c_y(x, y)}{10(\bar{c}_x(x, y) + \bar{c}_y(x, y))},
                                                                                                                                                                                                                                                                                                                                                                                                                                                                                                                                                           k_{0,4} = \frac{c_y(x,y)}{10(\bar{c}_x(x,y) + \bar{c}_y(x,y))}
                                                                    \bar{c}_y(x, y) - 5\bar{c}_x(x, y)
                                                                                                                                                                                                                                                                                                                                                                                                                                                                                                     \bar{c}_x(x, y) - 5\bar{c}_y(x, y)
                                                                                                                                                                                                                                                                                                                                                                                                                               k_{0,8} = \frac{c_x(x, y) - 5c_y(x, y)}{10(\bar{c}_x(x, y) + \bar{c}_y(x, y))}, \qquad k_{0,9} = -\frac{1}{20},
  k_{0.6} = \frac{c_y(x, y) - 5c_x(x, y)}{10(\bar{c}_x(x, y) + \bar{c}_y(x, y))}, \qquad k_{0.7} = -\frac{1}{20},
  k_{1,1} = -\frac{\bar{c}_y^{(0,1)}(x,y)\bar{c}_x(x,y)^2 - \bar{c}_y(x,y)(2\bar{c}_x^{(0,1)}(x,y) + \bar{c}_y^{(0,1)}(x,y) + c_x^{(1,0)}(x,y) + 2c_y^{(1,0)}(x,y))\bar{c}_x(x,y) + \bar{c}_y(x,y)^2\bar{c}_x^{(1,0)}(x,y)}{2}
                                                                                                                                                                                                                                                                                                                                                                         40\bar{c}_x(x, y)\bar{c}_y(x, y)(\bar{c}_x(x, y) + \bar{c}_y(x, y))
  k_{1,2} = \frac{\bar{c}_x(x, y)\bar{c}_y^{(0,1)}(x, y) + \bar{c}_y(x, y)(5\bar{c}_y^{(0,1)}(x, y) - 2\bar{c}_x^{(0,1)}(x, y))}{2\bar{c}_x^{(0,1)}(x, y) + \bar{c}_y(x, y)(5\bar{c}_y^{(0,1)}(x, y) - 2\bar{c}_x^{(0,1)}(x, y))}
                                                                                                                                                             20\bar{c}_{y}(x, y)(\bar{c}_{x}(x, y) + \bar{c}_{y}(x, y))
                                                            -\bar{c}_{y}^{(0,1)}(x,y)\bar{c}_{x}(x,y)^{2}+\bar{c}_{y}(x,y)(2\bar{c}_{x}^{(0,1)}(x,y)+\bar{c}_{y}^{(0,1)}(x,y)-\bar{c}_{x}^{(1,0)}(x,y)-2\bar{c}_{y}^{(1,0)}(x,y))\bar{c}_{x}(x,y)+\bar{c}_{y}(x,y)^{2}\bar{c}_{x}^{(1,0)}(x,y)
                                                                                                                                                                                                                                                                                                                                                                    40\bar{c}_x(x, y)\bar{c}_y(x, y)(\bar{c}_x(x, y) + \bar{c}_y(x, y))
  k_{1,4} = \frac{\bar{c}_y(x, y)\bar{c}_x^{(1,0)}(x, y) + \bar{c}_x(x, y)(5\bar{c}_x^{(1,0)}(x, y) - 2\bar{c}_y^{(1,0)}(x, y))}{2}
                                                                                                                                                             20\bar{c}_x(x, y)(\bar{c}_x(x, y) + \bar{c}_y(x, y))
                                                                                                         k_{1,6} = -\frac{\bar{c}_y(x,y)\bar{c}_x^{(1,0)}(x,y) + \bar{c}_x(x,y)(5\bar{c}_x^{(1,0)}(x,y) - 2\bar{c}_y^{(1,0)}(x,y))}{}
                                                                                                                                                                                                                                                                                       20\bar{c}_x(x, y)(\bar{c}_x(x, y) + \bar{c}_y(x, y))
  k_{1,7} = \frac{\bar{c}_y^{(0,1)}(x,y)\bar{c}_x(x,y)^2 + \bar{c}_y(x,y)(-2\bar{c}_x^{(0,1)}(x,y) - \bar{c}_y^{(0,1)}(x,y) + \bar{c}_x^{(1,0)}(x,y) + 2\bar{c}_y^{(1,0)}(x,y))\bar{c}_x(x,y) - \bar{c}_y(x,y)^2\bar{c}_x^{(1,0)}(x,y)}{\bar{c}_x(x,y)^2 + \bar{c}_y(x,y)(-2\bar{c}_x^{(0,1)}(x,y) - \bar{c}_y(x,y) + 2\bar{c}_y^{(1,0)}(x,y) + 2\bar{c}_y^{(1
                                                                                                                                                                                                                                                                                                                                                                  40\bar{c}_x(x, y)\bar{c}_y(x, y)(\bar{c}_x(x, y) + \bar{c}_y(x, y))
                                     = -\frac{\bar{c}_x(x,y)\bar{c}_y^{(0,1)}(x,y) + \bar{c}_y(x,y)(5\bar{c}_y^{(0,1)}(x,y) - 2\bar{c}_x^{(0,1)}(x,y))}{2}
                                                                                                                                                                             20\bar{c}_y(x, y)(\bar{c}_x(x, y) + \bar{c}_y(x, y))
                                                            \bar{c}_{y}^{(0,1)}(x,y)\bar{c}_{x}(x,y)^{2} - \bar{c}_{y}(x,y)(2\bar{c}_{x}^{(0,1)}(x,y) + \bar{c}_{y}^{(0,1)}(x,y) + \bar{c}_{x}^{(1,0)}(x,y) + 2\bar{c}_{y}^{(1,0)}(x,y))\bar{c}_{x}(x,y) + \bar{c}_{y}(x,y)^{2}\bar{c}_{x}^{(1,0)}(x,y)
                                                                                                                                                                                                                                                                                                                                                        40\bar{c}_x(x,y)\bar{c}_y(x,y)(\bar{c}_x(x,y)+\bar{c}_y(x,y))
                                                          \frac{1}{80\bar{c}_x(x,y)\bar{c}_y(x,y)(\bar{c}_x(x,y)+\bar{c}_y(x,y))}[\bar{c}_y(x,y)\bar{c}_x^{(1,0)}(x,y)(\bar{c}_y^{(0,1)}(x,y)+4\bar{c}_x^{(1,0)}(x,y)+2\bar{c}_y^{(1,0)}(x,y))+\bar{c}_x(x,y)(4\bar{c}_y^{(0,1)}(x,y)^2+2\bar{c}_x^{(0,1)}(x,y)\bar{c}_y^{(0,1)}(x,y)+4\bar{c}_x^{(1,0)}(x,y)+2\bar{c}_y^{(1,0)}(x,y)+2\bar{c}_y^{(1,0)}(x,y)+2\bar{c}_y^{(1,0)}(x,y)+2\bar{c}_y^{(1,0)}(x,y)+2\bar{c}_y^{(1,0)}(x,y)+2\bar{c}_y^{(1,0)}(x,y)+2\bar{c}_y^{(1,0)}(x,y)+2\bar{c}_y^{(1,0)}(x,y)+2\bar{c}_y^{(1,0)}(x,y)+2\bar{c}_y^{(1,0)}(x,y)+2\bar{c}_y^{(1,0)}(x,y)+2\bar{c}_y^{(1,0)}(x,y)+2\bar{c}_y^{(1,0)}(x,y)+2\bar{c}_y^{(1,0)}(x,y)+2\bar{c}_y^{(1,0)}(x,y)+2\bar{c}_y^{(1,0)}(x,y)+2\bar{c}_y^{(1,0)}(x,y)+2\bar{c}_y^{(1,0)}(x,y)+2\bar{c}_y^{(1,0)}(x,y)+2\bar{c}_y^{(1,0)}(x,y)+2\bar{c}_y^{(1,0)}(x,y)+2\bar{c}_y^{(1,0)}(x,y)+2\bar{c}_y^{(1,0)}(x,y)+2\bar{c}_y^{(1,0)}(x,y)+2\bar{c}_y^{(1,0)}(x,y)+2\bar{c}_y^{(1,0)}(x,y)+2\bar{c}_y^{(1,0)}(x,y)+2\bar{c}_y^{(1,0)}(x,y)+2\bar{c}_y^{(1,0)}(x,y)+2\bar{c}_y^{(1,0)}(x,y)+2\bar{c}_y^{(1,0)}(x,y)+2\bar{c}_y^{(1,0)}(x,y)+2\bar{c}_y^{(1,0)}(x,y)+2\bar{c}_y^{(1,0)}(x,y)+2\bar{c}_y^{(1,0)}(x,y)+2\bar{c}_y^{(1,0)}(x,y)+2\bar{c}_y^{(1,0)}(x,y)+2\bar{c}_y^{(1,0)}(x,y)+2\bar{c}_y^{(1,0)}(x,y)+2\bar{c}_y^{(1,0)}(x,y)+2\bar{c}_y^{(1,0)}(x,y)+2\bar{c}_y^{(1,0)}(x,y)+2\bar{c}_y^{(1,0)}(x,y)+2\bar{c}_y^{(1,0)}(x,y)+2\bar{c}_y^{(1,0)}(x,y)+2\bar{c}_y^{(1,0)}(x,y)+2\bar{c}_y^{(1,0)}(x,y)+2\bar{c}_y^{(1,0)}(x,y)+2\bar{c}_y^{(1,0)}(x,y)+2\bar{c}_y^{(1,0)}(x,y)+2\bar{c}_y^{(1,0)}(x,y)+2\bar{c}_y^{(1,0)}(x,y)+2\bar{c}_y^{(1,0)}(x,y)+2\bar{c}_y^{(1,0)}(x,y)+2\bar{c}_y^{(1,0)}(x,y)+2\bar{c}_y^{(1,0)}(x,y)+2\bar{c}_y^{(1,0)}(x,y)+2\bar{c}_y^{(1,0)}(x,y)+2\bar{c}_y^{(1,0)}(x,y)+2\bar{c}_y^{(1,0)}(x,y)+2\bar{c}_y^{(1,0)}(x,y)+2\bar{c}_y^{(1,0)}(x,y)+2\bar{c}_y^{(1,0)}(x,y)+2\bar{c}_y^{(1,0)}(x,y)+2\bar{c}_y^{(1,0)}(x,y)+2\bar{c}_y^{(1,0)}(x,y)+2\bar{c}_y^{(1,0)}(x,y)+2\bar{c}_y^{(1,0)}(x,y)+2\bar{c}_y^{(1,0)}(x,y)+2\bar{c}_y^{(1,0)}(x,y)+2\bar{c}_y^{(1,0)}(x,y)+2\bar{c}_y^{(1,0)}(x,y)+2\bar{c}_y^{(1,0)}(x,y)+2\bar{c}_y^{(1,0)}(x,y)+2\bar{c}_y^{(1,0)}(x,y)+2\bar{c}_y^{(1,0)}(x,y)+2\bar{c}_y^{(1,0)}(x,y)+2\bar{c}_y^{(1,0)}(x,y)+2\bar{c}_y^{(1,0)}(x,y)+2\bar{c}_y^{(1,0)}(x,y)+2\bar{c}_y^{(1,0)}(x,y)+2\bar{c}_y^{(1,0)}(x,y)+2\bar{c}_y^{(1,0)}(x,y)+2\bar{c}_y^{(1,0)}(x,y)+2\bar{c}_y^{(1,0)}(x,y)+2\bar{c}_y^{(1,0
  \bar{c}_{x}^{(1,0)}(x,y)\bar{c}_{y}^{(0,1)}(x,y) - 2\bar{c}_{y}(x,y)(\bar{c}_{x}^{(0,2)}(x,y) + 3\bar{c}_{y}^{(0,2)}(x,y) + \bar{c}_{x}^{(1,1)}(x,y) + \bar{c}_{y}^{(1,1)}(x,y) + 3\bar{c}_{x}^{(2,0)}(x,y) + \bar{c}_{y}^{(2,0)}(x,y))],
  k_{2,2} = \bar{c}_x(x, y)(\bar{c}_y(x, y)(\bar{c}_x^{(0,2)}(x, y) + 3\bar{c}_x^{(2,0)}(x, y)) - \bar{c}_x^{(0,1)}(x, y)\bar{c}_y^{(0,1)}(x, y)) - 2\bar{c}_y(x, y)\bar{c}_x^{(1,0)}(x, y)^2
                                                                                                                                                                                                                                                                    20\bar{c}_x(x, y)\bar{c}_y(x, y)(\bar{c}_x(x, y) + \bar{c}_y(x, y))
  k_{2,3} = \frac{1}{80\bar{c}_x(x,y)\bar{c}_y(x,y)(\bar{c}_x(x,y)+\bar{c}_y(x,y))} [\bar{c}_y(x,y)\bar{c}_x^{(1,0)}(x,y)(-\bar{c}_y^{(0,1)}(x,y)+4\bar{c}_x^{(1,0)}(x,y)+2\bar{c}_y^{(1,0)}(x,y)) + \bar{c}_x(x,y)(4\bar{c}_y^{(0,1)}(x,y)^2+2\bar{c}_x^{(0,1)}(x,y)\bar{c}_y^{(0,1)}(x,y)-2\bar{c}_y^{(0,1)}(x,y)\bar{c}_y^{(0,1)}(x,y)] + \bar{c}_x(x,y)\bar{c}_y(x,y)\bar{c}_y(x,y)\bar{c}_y(x,y)\bar{c}_y(x,y)\bar{c}_y(x,y)\bar{c}_y(x,y)\bar{c}_y(x,y)\bar{c}_y(x,y)\bar{c}_y(x,y)\bar{c}_y(x,y)\bar{c}_y(x,y)\bar{c}_y(x,y)\bar{c}_y(x,y)\bar{c}_y(x,y)\bar{c}_y(x,y)\bar{c}_y(x,y)\bar{c}_y(x,y)\bar{c}_y(x,y)\bar{c}_y(x,y)\bar{c}_y(x,y)\bar{c}_y(x,y)\bar{c}_y(x,y)\bar{c}_y(x,y)\bar{c}_y(x,y)\bar{c}_y(x,y)\bar{c}_y(x,y)\bar{c}_y(x,y)\bar{c}_y(x,y)\bar{c}_y(x,y)\bar{c}_y(x,y)\bar{c}_y(x,y)\bar{c}_y(x,y)\bar{c}_y(x,y)\bar{c}_y(x,y)\bar{c}_y(x,y)\bar{c}_y(x,y)\bar{c}_y(x,y)\bar{c}_y(x,y)\bar{c}_y(x,y)\bar{c}_y(x,y)\bar{c}_y(x,y)\bar{c}_y(x,y)\bar{c}_y(x,y)\bar{c}_y(x,y)\bar{c}_y(x,y)\bar{c}_y(x,y)\bar{c}_y(x,y)\bar{c}_y(x,y)\bar{c}_y(x,y)\bar{c}_y(x,y)\bar{c}_y(x,y)\bar{c}_y(x,y)\bar{c}_y(x,y)\bar{c}_y(x,y)\bar{c}_y(x,y)\bar{c}_y(x,y)\bar{c}_y(x,y)\bar{c}_y(x,y)\bar{c}_y(x,y)\bar{c}_y(x,y)\bar{c}_y(x,y)\bar{c}_y(x,y)\bar{c}_y(x,y)\bar{c}_y(x,y)\bar{c}_y(x,y)\bar{c}_y(x,y)\bar{c}_y(x,y)\bar{c}_y(x,y)\bar{c}_y(x,y)\bar{c}_y(x,y)\bar{c}_y(x,y)\bar{c}_y(x,y)\bar{c}_y(x,y)\bar{c}_y(x,y)\bar{c}_y(x,y)\bar{c}_y(x,y)\bar{c}_y(x,y)\bar{c}_y(x,y)\bar{c}_y(x,y)\bar{c}_y(x,y)\bar{c}_y(x,y)\bar{c}_y(x,y)\bar{c}_y(x,y)\bar{c}_y(x,y)\bar{c}_y(x,y)\bar{c}_y(x,y)\bar{c}_y(x,y)\bar{c}_y(x,y)\bar{c}_y(x,y)\bar{c}_y(x,y)\bar{c}_y(x,y)\bar{c}_y(x,y)\bar{c}_y(x,y)\bar{c}_y(x,y)\bar{c}_y(x,y)\bar{c}_y(x,y)\bar{c}_y(x,y)\bar{c}_y(x,y)\bar{c}_y(x,y)\bar{c}_y(x,y)\bar{c}_y(x,y)\bar{c}_y(x,y)\bar{c}_y(x,y)\bar{c}_y(x,y)\bar{c}_y(x,y)\bar{c}_y(x,y)\bar{c}_y(x,y)\bar{c}_y(x,y)\bar{c}_y(x,y)\bar{c}_y(x,y)\bar{c}_y(x,y)\bar{c}_y(x,y)\bar{c}_y(x,y)\bar{c}_y(x,y)\bar{c}_y(x,y)\bar{c}_y(x,y)\bar{c}_y(x,y)\bar{c}_y(x,y)\bar{c}_y(x,y)\bar{c}_y(x,y)\bar{c}_y(x,y)\bar{c}_y(x,y)\bar{c}_y(x,y)\bar{c}_y(x,y)\bar{c}_y(x,y)\bar{c}_y(x,y)\bar{c}_y(x,y)\bar{c}_y(x,y)\bar{c}_y(x,y)\bar{c}_y(x,y)\bar{c}_y(x,y)\bar{c}_y(x,y)\bar{c}_y(x,y)\bar{c}_y(x,y)\bar{c}_y(x,y)\bar{c}_y(x,y)\bar{c}_y(x,y)\bar{c}_y(x,y)\bar{c}_y(x,y)\bar{c}_y(x,y)\bar{c}_y(x,y)\bar{c}_y(x,y)\bar{c}_y(x,y)\bar{c}_y(x,y)\bar{c}_y(x,y)\bar{c}_y(x,y)\bar{c}_y(x,y)\bar{c}_y(x,y)\bar{c}_y(x,y)\bar{c}_y(x,y)\bar{c}_y(x,y)\bar{c}_y(x,y)\bar{c}_y(x,y)\bar{c}_y(x,y)\bar{c}_y(x,y)\bar{c}_y(x,y)\bar{c}_y(x,y)\bar{c}_y(x,y)\bar{c}_y(x,y)\bar{
    \bar{c}_{v}^{(1,0)}(x,y)\bar{c}_{v}^{(0,1)}(x,y) - 2\bar{c}_{v}(x,y)(\bar{c}_{v}^{(0,2)}(x,y) + 3\bar{c}_{v}^{(0,2)}(x,y) - \bar{c}_{v}^{(1,1)}(x,y) - \bar{c}_{v}^{(1,1)}(x,y) + 3\bar{c}_{v}^{(2,0)}(x,y) + \bar{c}_{v}^{(2,0)}(x,y))],
  k_{2,4} = \frac{\bar{c}_x(x,y)(\bar{c}_y(x,y)(3\bar{c}_y^{(0,2)}(x,y) + \bar{c}_y^{(2,0)}(x,y)) - 2\bar{c}_y^{(0,1)}(x,y)^2) - \bar{c}_y(x,y)\bar{c}_x^{(1,0)}(x,y)\bar{c}_y^{(1,0)}(x,y)}
                                                                                                                                                                                                                                                                      20\bar{c}_x(x, y)\bar{c}_y(x, y)(\bar{c}_x(x, y) + \bar{c}_y(x, y))
k_{2,5} = 0, \qquad k_{2,6} = \frac{\bar{c}_x(x,y)(\bar{c}_y(x,y)(3\bar{c}_y^{(0,2)}(x,y) + \bar{c}_y^{(2,0)}(x,y)) - 2\bar{c}_y^{(0,1)}(x,y)^2) - \bar{c}_y(x,y)\bar{c}_x^{(1,0)}(x,y)\bar{c}_y^{(1,0)}(x,y)}{2}
                                                                                                                                                                                                                                                                                                                                                                      20\bar{c}_x(x, y)\bar{c}_y(x, y)(\bar{c}_x(x, y) + \bar{c}_y(x, y))
  k_{2,7} = \frac{1}{80\bar{c}_x(x,y)\bar{c}_y(x,y)(\bar{c}_x(x,y) + \bar{c}_y(x,y))} \{\bar{c}_y(x,y)\bar{c}_x^{(1,0)}(x,y) - \bar{c}_y^{(0,1)}(x,y) + 4\bar{c}_x^{(1,0)}(x,y) + 2\bar{c}_y^{(1,0)}(x,y) + \bar{c}_x(x,y)(4\bar{c}_y^{(0,1)}(x,y)^2 + 2\bar{c}_x^{(0,1)}(x,y)\bar{c}_y^{(0,1)}(x,y) - 2\bar{c}_y^{(0,1)}(x,y)\bar{c}_y^{(0,1)}(x,y) + 2\bar{c}_x^{(0,1)}(x,y)\bar{c}_y^{(0,1)}(x,y) + 2\bar{c}_x^{(0,1)}(x,y)\bar{c}_y^{(0,1)}(x,y) + 2\bar{c}_x^{(0,1)}(x,y)\bar{c}_y^{(0,1)}(x,y)\bar{c}_y^{(0,1)}(x,y) + 2\bar{c}_x^{(0,1)}(x,y)\bar{c}_y^{(0,1)}(x,y) + 2\bar{c}_x^{(0,1)}(x,y)\bar{c}_y^{(0,1)}(x,y)\bar{c}_y^{(0,1)}(x,y)\bar{c}_y^{(0,1)}(x,y)\bar{c}_y^{(0,1)}(x,y)\bar{c}_y^{(0,1)}(x,y)\bar{c}_y^{(0,1)}(x,y)\bar{c}_y^{(0,1)}(x,y)\bar{c}_y^{(0,1)}(x,y)\bar{c}_y^{(0,1)}(x,y)\bar{c}_y^{(0,1)}(x,y)\bar{c}_y^{(0,1)}(x,y)\bar{c}_y^{(0,1)}(x,y)\bar{c}_y^{(0,1)}(x,y)\bar{c}_y^{(0,1)}(x,y)\bar{c}_y^{(0,1)}(x,y)\bar{c}_y^{(0,1)}(x,y)\bar{c}_y^{(0,1)}(x,y)\bar{c}_y^{(0,1)}(x,y)\bar{c}_y^{(0,1)}(x,y)\bar{c}_y^{(0,1)}(x,y)\bar{c}_y^{(0,1)}(x,y)\bar{c}_y^{(0,1)}(x,y)\bar{c}_y^{(0,1)}(x,y)\bar{c}_y^{(0,1)}(x,y)\bar{c}_y^{(0,1)}(x,y)\bar{c}_y^{(0,1)}(x,y)\bar{c}_y^{(0,1)}(x,y)\bar{c}_y^{(0,1)}(x,y)\bar{c}_y^{(0,1)}(x,y)\bar{c}_y^{(0,1)}(x,y)\bar{c}_y^{(0,1)}(x,y)\bar{c}_y^{(0,1)}(x,y)\bar{c}_y^{(0,1)}(x,y)\bar{c}_y^{(0,1)}(x,y)\bar{c}_y^{(0,1)}(x,y)\bar{c}_y^{(0,1)}(x,y)\bar{c}_y^{(0,1)}(x,y)\bar{c}_y^{(0,1)}(x,y)\bar{c}_y^{(0,1)}(x,y)\bar{c}_y^{(0,1)}(x,y)\bar{c}_y^{(0,1)}(x,y)\bar{c}_y^{(0,1)}(x,y)\bar{c}_y^{(0,1)}(x,y)\bar{c}_y^{(0,1)}(x,y)\bar{c}_y^{(0,1)}(x,y)\bar{c}_y^{(0,1)}(x,y)\bar{c}_y^{(0,1)}(x,y)\bar{c}_y^{(0,1)}(x,y)\bar{c}_y^{(0,1)}(x,y)\bar{c}_y^{(0,1)}(x,y)\bar{c}_y^{(0,1)}(x,y)\bar{c}_y^{(0,1)}(x,y)\bar{c}_y^{(0,1)}(x,y)\bar{c}_y^{(0,1)}(x,y)\bar{c}_y^{(0,1)}(x,y)\bar{c}_y^{(0,1)}(x,y)\bar{c}_y^{(0,1)}(x,y)\bar{c}_y^{(0,1)}(x,y)\bar{c}_y^{(0,1)}(x,y)\bar{c}_y^{(0,1)}(x,y)\bar{c}_y^{(0,1)}(x,y)\bar{c}_y^{(0,1)}(x,y)\bar{c}_y^{(0,1)}(x,y)\bar{c}_y^{(0,1)}(x,y)\bar{c}_y^{(0,1)}(x,y)\bar{c}_y^{(0,1)}(x,y)\bar{c}_y^{(0,1)}(x,y)\bar{c}_y^{(0,1)}(x,y)\bar{c}_y^{(0,1)}(x,y)\bar{c}_y^{(0,1)}(x,y)\bar{c}_y^{(0,1)}(x,y)\bar{c}_y^{(0,1)}(x,y)\bar{c}_y^{(0,1)}(x,y)\bar{c}_y^{(0,1)}(x,y)\bar{c}_y^{(0,1)}(x,y)\bar{c}_y^{(0,1)}(x,y)\bar{c}_y^{(0,1)}(x,y)\bar{c}_y^{(0,1)}(x,y)\bar{c}_y^{(0,1)}(x,y)\bar{c}_y^{(0,1)}(x,y)\bar{c}_y^{(0,1)}(x,y)\bar{c}_y^
    \bar{c}_{x}^{(1,0)}(x,y)\bar{c}_{y}^{(0,1)}(x,y) - 2\bar{c}_{y}(x,y)(\bar{c}_{x}^{(0,2)}(x,y) + 3\bar{c}_{y}^{(0,2)}(x,y) - \bar{c}_{x}^{(1,1)}(x,y) - \bar{c}_{y}^{(1,1)}(x,y) + 3\bar{c}_{x}^{(2,0)}(x,y) + \bar{c}_{y}^{(2,0)}(x,y))],
                                                        \bar{c}_x(x,y)(\bar{c}_y(x,y)(\bar{c}_x^{(0,2)}(x,y)+3\bar{c}_x^{(2,0)}(x,y))-\bar{c}_x^{(0,1)}(x,y)\bar{c}_y^{(0,1)}(x,y))-2\bar{c}_y(x,y)\bar{c}_x^{(1,0)}(x,y)^2
                                                                                                                                                                                                                                                                    20\bar{c}_x(x, y)\bar{c}_y(x, y)(\bar{c}_x(x, y) + \bar{c}_y(x, y))
k_{2,9} = \frac{1}{80\bar{c}_x(x,y)\bar{c}_y(x,y)(\bar{c}_x(x,y) + \bar{c}_y(x,y))} (\bar{c}_y(x,y)\bar{c}_x^{(1,0)}(x,y)\bar{c}_y^{(0,1)}(x,y) + 4\bar{c}_x^{(1,0)}(x,y) + 2\bar{c}_y^{(1,0)}(x,y)) + \bar{c}_x(x,y)(4\bar{c}_y^{(0,1)}(x,y)^2 + 2\bar{c}_x^{(0,1)}(x,y)\bar{c}_y^{(0,1)}(x,y) + 4\bar{c}_x^{(1,0)}(x,y) + 2\bar{c}_y^{(1,0)}(x,y)\bar{c}_y^{(0,1)}(x,y) + 2\bar{c}_x^{(0,1)}(x,y)\bar{c}_y^{(0,1)}(x,y) + 2\bar{c}_y^{(0,1)}(x,y)\bar{c}_y^{(0,1)}(x,y) + 2\bar{c}_y^{(0,1)}(x,y)\bar{c}_y^{(0,1)}(x,y)\bar{c}_y^{(0,1)}(x,y) + 2\bar{c}_y^{(0,1)}(x,y)\bar{c}_y^{(0,1)}(x,y) + 2\bar{c}_y^{(0,1)}(x,y)\bar{c}_y^{(0,1)}(x,y)\bar{c}_y^{(0,1)}(x,y) + 2\bar{c}_y^{(0,1)}(x,y)\bar{c}_y^{(0,1)}(x,y)\bar{c}_y^{(0,1)}(x,y)\bar{c}_y^{(0,1)}(x,y) + 2\bar{c}_y^{(0,1)}(x,y)\bar{c}_y^{(0,1)}(x,y)\bar{c}_y^{(0,1)}(x,y) + 2\bar{c}_y^{(0,1)}(x,y)\bar{c}_y^{(0,1)}(x,y)\bar{c}_y^{(0,1)}(x,y)\bar{c}_y^{(0,1)}(x,y)\bar{c}_y^{(0,1)}(x,y)\bar{c}_y^{(0,1)}(x,y)\bar{c}_y^{(0,1)}(x,y)\bar{c}_y^{(0,1)}(x,y)\bar{c}_y^{(0,1)}(x,y)\bar{c}_y^{(0,1)}(x,y)\bar{c}_y^{(0,1)}(x,y)\bar{c}_y^{(0,1)}(x,y)\bar{c}_y^{(0,1)}(x,y)\bar{c}_y^{(0,1)}(x,y)\bar{c}_y^{(0,1)}(x,y)\bar{c}_y^{(0,1)}(x,y)\bar{c}_y^{(0,1)}(x,y)\bar{c}_y^{(0,1)}(x,y)\bar{c}_y^{(0,1)}(x,y)\bar{c}_y^{(0,1)}(x,y)\bar{c}_y^{(0,1)}(x,y)\bar{c}_y^{(0,1)}(x,y)\bar{c}_y^{(0,1)}(x,y)\bar{c}_y^{(0,1)}(x,y)\bar{c}_y^{(0,1)}(x,y)\bar{c}_y^{(0,1)}(x,y)\bar{c}_y^{(0,1)}(x,y)\bar{c}_y^{(0,1)}(x,y)\bar{c}_y^{(0,1)}(x,y)\bar{c}_y^{(0,1)}(x,y)\bar{c}_y^{(0,1)}(x,y)\bar{c}_y^{(0,1)}(x,y)\bar{c}_y^{(0,1)}(x,y)\bar{c}_y^{(0,1)}(x,y)\bar{c}_y^{(0,1)}(x,y)\bar{c}_y^{(0,1)}(x,y)\bar{c}_y^{(0,1)}(x,y)\bar{c}_y^{(0,1)}(x,y)\bar{c}_y^{(0,1)}(x,y)\bar{c}_y^{(0,1)}(x,y)\bar{c}_y^{(0,1)}(x,y)\bar{c}_y^{(0,1)}(x,y)\bar{c}_y^{(0,1)}(x,y)\bar{c}_y^{(0,1)}(x,y)\bar{c}_y^{(0,1)}(x,y)\bar{c}_y^{(0,1)}(x,y)\bar{c}_y^{(0,1)}(x,y)\bar{c}_y^{(0,1)}(x,y)\bar{c}_y^{(0,1)}(x,y)\bar{c}_y^{(0,1)}(x,y)\bar{c}_y^{(0,1)}(x,y)\bar{c}_y^{(0,1)}(x,y)\bar{c}_y^{(0,1)}(x,y)\bar{c}_y^{(0,1)}(x,y)\bar{c}_y^{(0,1)}(x,y)\bar{c}_y^{(0,1)}(x,y)\bar{c}_y^{(0,1)}(x,y)\bar{c}_y^{(0,1)}(x,y)\bar{c}_y^{(0,1)}(x,y)\bar{c}_y^{(0,1)}(x,y)\bar{c}_y^{(0,1)}(x,y)\bar{c}_y^{(0,1)}(x,y)\bar{c}_y^{(0,1)}(x,y)\bar{c}_y^{(0,1)}(x,y)\bar{c}_y^{(0,1)}(x,y)\bar{c}_y^{(0,1)}(x,y)\bar{c}_y^{(0,1)}(x,y)\bar{c}_y^{(0,1)}(x,y)\bar{c}_y^{(0,1)}(x,y)\bar{c}_y^{(0,1)}(x,y)\bar{c}_y^{(0,1
  \bar{c}_{v}^{(1,0)}(x,y)\bar{c}_{v}^{(0,1)}(x,y) - 2\bar{c}_{v}(x,y)(\bar{c}_{v}^{(0,2)}(x,y) + 3\bar{c}_{v}^{(0,2)}(x,y) + \bar{c}_{v}^{(1,1)}(x,y) + \bar{c}_{v}^{(1,1)}(x,y) + 3\bar{c}_{v}^{(2,0)}(x,y) + \bar{c}_{v}^{(2,0)}(x,y))],
  k_{3,1} = \frac{1}{480\bar{c}_x(x,y)\bar{c}_y(x,y)(\bar{c}_x(x,y) + \bar{c}_y(x,y))} [\bar{c}_x(x,y)(\bar{c}_y(x,y)(4\bar{c}_x^{(0,3)}(x,y) + \bar{c}_y^{(0,3)}(x,y) + 6\bar{c}_x^{(1,2)}(x,y) + 6\bar{c}_x^{(1,2)}(x,y) + 6\bar{c}_x^{(2,1)}(x,y) + 6\bar{c}_x^{(2,1)}(x,y
  6\bar{c}_{v}^{(2,1)}(x,y) + \bar{c}_{x}^{(3,0)}(x,y) + 4\bar{c}_{v}^{(3,0)}(x,y)) - \bar{c}_{v}^{(0,1)}(x,y) \\ 6\bar{c}_{x}^{(0,2)}(x,y) + \bar{c}_{v}^{(0,2)}(x,y) + 6\bar{c}_{x}^{(1,1)}(x,y) + 4\bar{c}_{v}^{(1,1)}(x,y) + 3\bar{c}_{x}^{(2,0)}(x,y)) \\ - \bar{c}_{v}^{(0,1)}(x,y) + \bar{c}_{v}^{(0,2)}(x,y) + \bar{c}_{v}^{(0,2)}(x,y) + 6\bar{c}_{x}^{(1,1)}(x,y) + 4\bar{c}_{v}^{(1,1)}(x,y) + 3\bar{c}_{x}^{(2,0)}(x,y) \\ - \bar{c}_{v}^{(0,1)}(x,y) + \bar{c}_{v}^{(0,2)}(x,y) + \bar{c}_{v}^{(0,2)}(x,y) + 6\bar{c}_{x}^{(0,2)}(x,y) + 6\bar{c}_{x}^{(0,2)}(x,y) \\ - \bar{c}_{v}^{(0,2)}(x,y) + \bar{c}_{v}^{(0,2)}(x,y) + \bar{c}_{v}^{(0,2)}(x,y) + \bar{c}_{v}^{(0,2)}(x,y) \\ - \bar{c}_{v}^{(0,2)}(x,y) + \bar{c}_{v}^{(0,2)}(x,y) + \bar{c}_{v}^{(0,2)}(x,y) + \bar{c}_{v}^{(0,2)}(x,y) \\ - \bar{c}_{v}^{(0,2)}(x,y) + \bar{c}_{v}^{(0,2)}(x,y) + \bar{c}_{v}^{(0,2)}(x,y) + \bar{c}_{v}^{(0,2)}(x,y) \\ - \bar{c}_{v}^{(0,2)}(x,y) + \bar{c}_{v}^{(0,2)}(x,y) + \bar{c}_{v}^{(0,2)}(x,y) + \bar{c}_{v}^{(0,2)}(x,y) \\ - \bar{c}_{v}^{(0,2)}(x,y) + \bar{c}_{v}^{(0,2)}(x,y) + \bar{c}_{v}^{(0,2)}(x,y) + \bar{c}_{v}^{(0,2)}(x,y) \\ - \bar{c}_{v}^{(0,2)}(x,y) + \bar{c}_{v}^{(0,2)}(x,y) + \bar{c}_{v}^{(0,2)}(x,y) + \bar{c}_{v}^{(0,2)}(x,y) + \bar{c}_{v}^{(0,2)}(x,y) + \bar{c}_{v}^{(0,2)}(x,y) \\ - \bar{c}_{v}^{(0,2)}(x,y) + \bar{c}_{v}^{(0,2)}(x,y)
  \bar{c}_y(x,y)\bar{c}_x^{(1,0)}(x,y)(3\bar{c}_y^{(0,2)}(x,y)+4\bar{c}_x^{(1,1)}(x,y)+6\bar{c}_y^{(1,1)}(x,y)+\bar{c}_x^{(2,0)}(x,y)+6\bar{c}_y^{(2,0)}(x,y))],
  k_{3,2} = \frac{4\bar{c}_y(x,y)\bar{c}_x^{(1,0)}(x,y)\bar{c}_x^{(1,1)}(x,y) + \bar{c}_x(x,y)(\bar{c}_y^{(0,1)}(x,y)(6\bar{c}_x^{(0,2)}(x,y) - 5\bar{c}_y^{(0,2)}(x,y) + 3\bar{c}_x^{(2,0)}(x,y)) + \bar{c}_y(x,y)(-4\bar{c}_x^{(0,3)}(x,y) + 5\bar{c}_y^{(0,3)}(x,y) - 6\bar{c}_x^{(2,1)}(x,y)))}{2(1+|c_x|^2)}
                                                                                                                                                                                                                                                                                                                                                                                                                                                                                              240\bar{c}_x(x, y)\bar{c}_y(x, y)(\bar{c}_x(x, y) + \bar{c}_y(x, y))
  k_{3,3} = \frac{1}{480\bar{c}_x(x,y)\bar{c}_y(x,y)(\bar{c}_x(x,y) + \bar{c}_y(x,y))} [\bar{c}_y(x,y)\bar{c}_x^{(1,0)}(x,y)(3\bar{c}_y^{(0,2)}(x,y) - 4\bar{c}_x^{(1,1)}(x,y) - 6\bar{c}_y^{(1,1)}(x,y) + \bar{c}_x^{(2,0)}(x,y) + 6\bar{c}_y^{(2,0)}(x,y))]
  \bar{c}_x(x,y)(\bar{c}_v^{(0,1)}(x,y)(6\bar{c}_x^{(0,2)}(x,y)+\bar{c}_v^{(0,2)}(x,y)-6\bar{c}_x^{(1,1)}(x,y)-4\bar{c}_y^{(1,1)}(x,y)+3\bar{c}_x^{(2,0)}(x,y))+\bar{c}_y(x,y)(-4\bar{c}_x^{(0,3)}(x,y)-\bar{c}_y^{(0,3)}(x,y)+2\bar{c}_y^{(0,2)}(x,y))+2\bar{c}_y(x,y)(-4\bar{c}_x^{(0,2)}(x,y)+2\bar{c}_y^{(0,2)}(x,y)+2\bar{c}_y^{(0,2)}(x,y)+2\bar{c}_y^{(0,2)}(x,y)+2\bar{c}_y^{(0,2)}(x,y)+2\bar{c}_y^{(0,2)}(x,y)+2\bar{c}_y^{(0,2)}(x,y)+2\bar{c}_y^{(0,2)}(x,y)+2\bar{c}_y^{(0,2)}(x,y)+2\bar{c}_y^{(0,2)}(x,y)+2\bar{c}_y^{(0,2)}(x,y)+2\bar{c}_y^{(0,2)}(x,y)+2\bar{c}_y^{(0,2)}(x,y)+2\bar{c}_y^{(0,2)}(x,y)+2\bar{c}_y^{(0,2)}(x,y)+2\bar{c}_y^{(0,2)}(x,y)+2\bar{c}_y^{(0,2)}(x,y)+2\bar{c}_y^{(0,2)}(x,y)+2\bar{c}_y^{(0,2)}(x,y)+2\bar{c}_y^{(0,2)}(x,y)+2\bar{c}_y^{(0,2)}(x,y)+2\bar{c}_y^{(0,2)}(x,y)+2\bar{c}_y^{(0,2)}(x,y)+2\bar{c}_y^{(0,2)}(x,y)+2\bar{c}_y^{(0,2)}(x,y)+2\bar{c}_y^{(0,2)}(x,y)+2\bar{c}_y^{(0,2)}(x,y)+2\bar{c}_y^{(0,2)}(x,y)+2\bar{c}_y^{(0,2)}(x,y)+2\bar{c}_y^{(0,2)}(x,y)+2\bar{c}_y^{(0,2)}(x,y)+2\bar{c}_y^{(0,2)}(x,y)+2\bar{c}_y^{(0,2)}(x,y)+2\bar{c}_y^{(0,2)}(x,y)+2\bar{c}_y^{(0,2)}(x,y)+2\bar{c}_y^{(0,2)}(x,y)+2\bar{c}_y^{(0,2)}(x,y)+2\bar{c}_y^{(0,2)}(x,y)+2\bar{c}_y^{(0,2)}(x,y)+2\bar{c}_y^{(0,2)}(x,y)+2\bar{c}_y^{(0,2)}(x,y)+2\bar{c}_y^{(0,2)}(x,y)+2\bar{c}_y^{(0,2)}(x,y)+2\bar{c}_y^{(0,2)}(x,y)+2\bar{c}_y^{(0,2)}(x,y)+2\bar{c}_y^{(0,2)}(x,y)+2\bar{c}_y^{(0,2)}(x,y)+2\bar{c}_y^{(0,2)}(x,y)+2\bar{c}_y^{(0,2)}(x,y)+2\bar{c}_y^{(0,2)}(x,y)+2\bar{c}_y^{(0,2)}(x,y)+2\bar{c}_y^{(0,2)}(x,y)+2\bar{c}_y^{(0,2)}(x,y)+2\bar{c}_y^{(0,2)}(x,y)+2\bar{c}_y^{(0,2)}(x,y)+2\bar{c}_y^{(0,2)}(x,y)+2\bar{c}_y^{(0,2)}(x,y)+2\bar{c}_y^{(0,2)}(x,y)+2\bar{c}_y^{(0,2)}(x,y)+2\bar{c}_y^{(0,2)}(x,y)+2\bar{c}_y^{(0,2)}(x,y)+2\bar{c}_y^{(0,2)}(x,y)+2\bar{c}_y^{(0,2)}(x,y)+2\bar{c}_y^{(0,2)}(x,y)+2\bar{c}_y^{(0,2)}(x,y)+2\bar{c}_y^{(0,2)}(x,y)+2\bar{c}_y^{(0,2)}(x,y)+2\bar{c}_y^{(0,2)}(x,y)+2\bar{c}_y^{(0,2)}(x,y)+2\bar{c}_y^{(0,2)}(x,y)+2\bar{c}_y^{(0,2)}(x,y)+2\bar{c}_y^{(0,2)}(x,y)+2\bar{c}_y^{(0,2)}(x,y)+2\bar{c}_y^{(0,2)}(x,y)+2\bar{c}_y^{(0,2)}(x,y)+2\bar{c}_y^{(0,2)}(x,y)+2\bar{c}_y^{(0,2)}(x,y)+2\bar{c}_y^{(0,2)}(x,y)+2\bar{c}_y^{(0,2)}(x,y)+2\bar{c}_y^{(0,2)}(x,y)+2\bar{c}_y^{(0,2)}(x,y)+2\bar{c}_y^{(0,2)}(x,y)+2\bar{c}_y^{(0,2)}(x,y)+2\bar{c}_y^{(0,2)}(x,y)+2\bar{c}_y^{(0,2)}(x,y)+2\bar{c}_y^{(0,2)}(x,y)+2\bar{c}_y^{(0
  6\bar{c}_{x}^{(1,2)}(x,y)+6\bar{c}_{y}^{(1,2)}(x,y)-6\bar{c}_{x}^{(2,1)}(x,y)-6\bar{c}_{y}^{(2,1)}(x,y)+\bar{c}_{x}^{(3,0)}(x,y)+4\bar{c}_{y}^{(3,0)}(x,y)))],
                                                        4\bar{c}_x(x,y)\bar{c}_x^{(0,1)}(x,y)\bar{c}_x^{(1,1)}(x,y) + \bar{c}_y(x,y)(3\bar{c}_y^{(0,2)}(x,y)\bar{c}_x^{(1,0)}(x,y) + (6\bar{c}_y^{(2,0)}(x,y) - 5\bar{c}_x^{(2,0)}(x,y))\bar{c}_x^{(1,0)}(x,y) + \bar{c}_x(x,y)(-6\bar{c}_y^{(1,2)}(x,y) + 5\bar{c}_x^{(3,0)}(x,y) - 4\bar{c}_y^{(3,0)}(x,y)))
                                                                                                                                                                                                                                                                                                                                                                                                                                                                                                                                        240\bar{c}_x(x, y)\bar{c}_y(x, y)(\bar{c}_x(x, y) + \bar{c}_y(x, y))
  k_{3,6} = \frac{\bar{c}_y(x,y)(-3\bar{c}_y^{(0,2)}(x,y)\bar{c}_x^{(1,0)}(x,y) + (5\bar{c}_x^{(2,0)}(x,y) - 6\bar{c}_y^{(2,0)}(x,y))\bar{c}_x^{(1,0)}(x,y) + \bar{c}_x(x,y)(6\bar{c}_y^{(1,2)}(x,y) - 5\bar{c}_x^{(3,0)}(x,y) + 4\bar{c}_y^{(3,0)}(x,y)) - 4\bar{c}_x(x,y)\bar{c}_y^{(0,1)}(x,y)\bar{c}_y^{(1,1)}(x,y) + 2\bar{c}_x(x,y)\bar{c}_y^{(0,1)}(x,y) + 2\bar{c}_x
                                                                                                                                                                                                                                                                                                                                                                                                                                                                                                                                        240\bar{c}_x(x, y)\bar{c}_y(x, y)(\bar{c}_x(x, y) + \bar{c}_y(x, y))
  k_{3,7} = \frac{1}{480\bar{c}_x(x,y)\bar{c}_y(x,y)(\bar{c}_x(x,y) + \bar{c}_y(x,y))} [\bar{c}_x(x,y)(\bar{c}_y^{(0,1)}(x,y)(6\bar{c}_x^{(0,2)}(x,y) + \bar{c}_y^{(0,2)}(x,y) - 6\bar{c}_x^{(1,1)}(x,y) - 4\bar{c}_y^{(1,1)}(x,y) + 3\bar{c}_x^{(2,0)}(x,y)) + 2\bar{c}_y^{(0,2)}(x,y) + 2\bar{c}_y^{(
  \bar{c}_y(x,y)(-4\bar{c}_x^{(0,3)}(x,y) - \bar{c}_y^{(0,3)}(x,y) + 6\bar{c}_x^{(1,2)}(x,y) + 6\bar{c}_y^{(1,2)}(x,y) - 6\bar{c}_y^{(2,1)}(x,y) - 6\bar{c}_y^{(2,1)}(x,y) + \bar{c}_x^{(3,0)}(x,y) + 4\bar{c}_y^{(3,0)}(x,y))) - \bar{c}_y(x,y)(-4\bar{c}_x^{(0,3)}(x,y) - \bar{c}_y(x,y)) - \bar{c}_y(x,y)(-4\bar{c}_x^{(0,3)}(x,y) - \bar{c}_y(x,y)) - \bar{c}_y(x,y)(-4\bar{c}_x^{(0,3)}(x,y) - \bar{c}_y(x,y)) - \bar{c}_y(x,y)(-4\bar{c}_x(x,y) - \bar{c}_y(x,y)) - \bar{c}_y(x,y)(-4\bar{c}_x(x,y) - \bar{c}_y(x,y)) - \bar{c}_y(x,y)(-4\bar{c}_x(x,y) - \bar{c}_y(x,y)) - \bar{c}_y(x,y)(-4\bar{c}_x(x,y) - \bar{c}_y(x,y) - \bar{c}_y(x,y)) - \bar{c}_y(x,y)(-4\bar{c}_x(x,y) - \bar{c}_y(x,y) - \bar{c}_y(x,y)) - \bar{c}_y(x,y)(-4\bar{c}_x(x,y) - \bar{c}_y(x,y) - \bar{c}_y(x,y)) - \bar{c}_y(x,y)(-4\bar{c}_y(x,y) - \bar{c}_y(x,y) - \bar{c}_y(x,y) - \bar{c}_y(x,y)) - \bar{c}_y(x,y)(-4\bar{c}_y(x,y) - \bar{c}_y(x,y) - \bar{c}_y(x,y)) - \bar{c}_y(x,y)(-4\bar{c}_y(x,y) - \bar{c}_y(x,y) - \bar{c}_y
  \bar{c}_y(x,y)\bar{c}_x^{(1,0)}(x,y)(3\bar{c}_y^{(0,2)}(x,y)-4\bar{c}_x^{(1,1)}(x,y)-6\bar{c}_y^{(1,1)}(x,y)+\bar{c}_x^{(2,0)}(x,y)+6\bar{c}_y^{(2,0)}(x,y))],
  k_{3.8} = \frac{\bar{c}_x(x,y)(\bar{c}_y^{(0,1)}(x,y)(-6\bar{c}_x^{(0,2)}(x,y) + 5\bar{c}_y^{(0,2)}(x,y) - 3\bar{c}_x^{(2,0)}(x,y)) + \bar{c}_y(x,y)(4\bar{c}_x^{(0,3)}(x,y) - 5\bar{c}_y^{(0,3)}(x,y) + 6\bar{c}_x^{(2,1)}(x,y))) - 4\bar{c}_y(x,y)\bar{c}_x^{(1,0)}(x,y)\bar{c}_x^{(1,1)}(x,y) + 2\bar{c}_y(x,y)\bar{c}_x^{(1,0)}(x,y) + 2\bar{c}_y(x,y)\bar{c}_x^{(1,0)
                                                                                                                                                                                                                                                                                                                                                                                                                                                                                                240\bar{c}_x(x, y)\bar{c}_y(x, y)(\bar{c}_x(x, y) + \bar{c}_y(x, y))
  k_{3,9} = \frac{1}{480\bar{c}_x(x,y)\bar{c}_y(x,y)(\bar{c}_x(x,y) + \bar{c}_y(x,y))} \{\bar{c}_y(x,y)\bar{c}_x^{(1,0)}(x,y)(3\bar{c}_y^{(0,2)}(x,y) + 4\bar{c}_x^{(1,1)}(x,y) + 6\bar{c}_y^{(1,1)}(x,y) + \bar{c}_x^{(2,0)}(x,y) + 6\bar{c}_y^{(2,0)}(x,y)) + 4\bar{c}_x^{(1,1)}(x,y) + \bar{c}_x^{(2,0)}(x,y) + \bar
  \bar{c}_x(x,y)(\bar{c}_v^{(0,1)}(x,y)(6\bar{c}_x^{(0,2)}(x,y)+\bar{c}_v^{(0,2)}(x,y)+\bar{c}_v^{(0,2)}(x,y)+6\bar{c}_x^{(1,1)}(x,y)+4\bar{c}_v^{(1,1)}(x,y)+3\bar{c}_x^{(2,0)}(x,y))-\bar{c}_y(x,y)(4\bar{c}_x^{(0,3)}(x,y)+\bar{c}_v^{(0,3)}(x,y)+\bar{c}_y^{(0,3)}(x,y)+\bar{c}_y^{(0,3)}(x,y)+\bar{c}_y^{(0,3)}(x,y)+\bar{c}_y^{(0,3)}(x,y)+\bar{c}_y^{(0,3)}(x,y)+\bar{c}_y^{(0,3)}(x,y)+\bar{c}_y^{(0,3)}(x,y)+\bar{c}_y^{(0,3)}(x,y)+\bar{c}_y^{(0,3)}(x,y)+\bar{c}_y^{(0,3)}(x,y)+\bar{c}_y^{(0,3)}(x,y)+\bar{c}_y^{(0,3)}(x,y)+\bar{c}_y^{(0,3)}(x,y)+\bar{c}_y^{(0,3)}(x,y)+\bar{c}_y^{(0,3)}(x,y)+\bar{c}_y^{(0,3)}(x,y)+\bar{c}_y^{(0,3)}(x,y)+\bar{c}_y^{(0,3)}(x,y)+\bar{c}_y^{(0,3)}(x,y)+\bar{c}_y^{(0,3)}(x,y)+\bar{c}_y^{(0,3)}(x,y)+\bar{c}_y^{(0,3)}(x,y)+\bar{c}_y^{(0,3)}(x,y)+\bar{c}_y^{(0,3)}(x,y)+\bar{c}_y^{(0,3)}(x,y)+\bar{c}_y^{(0,3)}(x,y)+\bar{c}_y^{(0,3)}(x,y)+\bar{c}_y^{(0,3)}(x,y)+\bar{c}_y^{(0,3)}(x,y)+\bar{c}_y^{(0,3)}(x,y)+\bar{c}_y^{(0,3)}(x,y)+\bar{c}_y^{(0,3)}(x,y)+\bar{c}_y^{(0,3)}(x,y)+\bar{c}_y^{(0,3)}(x,y)+\bar{c}_y^{(0,3)}(x,y)+\bar{c}_y^{(0,3)}(x,y)+\bar{c}_y^{(0,3)}(x,y)+\bar{c}_y^{(0,3)}(x,y)+\bar{c}_y^{(0,3)}(x,y)+\bar{c}_y^{(0,3)}(x,y)+\bar{c}_y^{(0,3)}(x,y)+\bar{c}_y^{(0,3)}(x,y)+\bar{c}_y^{(0,3)}(x,y)+\bar{c}_y^{(0,3)}(x,y)+\bar{c}_y^{(0,3)}(x,y)+\bar{c}_y^{(0,3)}(x,y)+\bar{c}_y^{(0,3)}(x,y)+\bar{c}_y^{(0,3)}(x,y)+\bar{c}_y^{(0,3)}(x,y)+\bar{c}_y^{(0,3)}(x,y)+\bar{c}_y^{(0,3)}(x,y)+\bar{c}_y^{(0,3)}(x,y)+\bar{c}_y^{(0,3)}(x,y)+\bar{c}_y^{(0,3)}(x,y)+\bar{c}_y^{(0,3)}(x,y)+\bar{c}_y^{(0,3)}(x,y)+\bar{c}_y^{(0,3)}(x,y)+\bar{c}_y^{(0,3)}(x,y)+\bar{c}_y^{(0,3)}(x,y)+\bar{c}_y^{(0,3)}(x,y)+\bar{c}_y^{(0,3)}(x,y)+\bar{c}_y^{(0,3)}(x,y)+\bar{c}_y^{(0,3)}(x,y)+\bar{c}_y^{(0,3)}(x,y)+\bar{c}_y^{(0,3)}(x,y)+\bar{c}_y^{(0,3)}(x,y)+\bar{c}_y^{(0,3)}(x,y)+\bar{c}_y^{(0,3)}(x,y)+\bar{c}_y^{(0,3)}(x,y)+\bar{c}_y^{(0,3)}(x,y)+\bar{c}_y^{(0,3)}(x,y)+\bar{c}_y^{(0,3)}(x,y)+\bar{c}_y^{(0,3)}(x,y)+\bar{c}_y^{(0,3)}(x,y)+\bar{c}_y^{(0,3)}(x,y)+\bar{c}_y^{(0,3)}(x,y)+\bar{c}_y^{(0,3)}(x,y)+\bar{c}_y^{(0,3)}(x,y)+\bar{c}_y^{(0,3)}(x,y)+\bar{c}_y^{(0,3)}(x,y)+\bar{c}_y^{(0,3)}(x,y)+\bar{c}_y^{(0,3)}(x,y)+\bar{c}_y^{(0,3)}(x,y)+\bar{c}_y^{(0,3)}(x,y)+\bar{c}_y^{(0,3)}(x,y)+\bar{c}_y^{(0,3)}(x,y)+\bar{c}_y^{(0,3)}(x,y)+\bar{c}_y^{(0,3)}(x,y)+\bar{c}_y^{(0,3)}(x,y)+\bar{c}_y^{(0,3)}(x,y)+\bar{c}_y^{(0,3)}(x,y)+\bar{c}_y^{(0,3)}
```

```
6\bar{c}_{r}^{(1,2)}(x,y) + 6\bar{c}_{v}^{(1,2)}(x,y) + 6\bar{c}_{r}^{(2,1)}(x,y) + 6\bar{c}_{v}^{(2,1)}(x,y) + \bar{c}_{r}^{(3,0)}(x,y) + 4\bar{c}_{v}^{(3,0)}(x,y)))],
k_{4,1} = \frac{1}{960\bar{c}_x(x,y)\bar{c}_y(x,y)(\bar{c}_x(x,y) + \bar{c}_y(x,y))} [\bar{c}_y(x,y)\bar{c}_x^{(1,0)}(x,y)(\bar{c}_y^{(0,3)}(x,y) + 2(2\bar{c}_x^{(1,2)}(x,y) + 3\bar{c}_y^{(2,1)}(x,y) + \bar{c}_x^{(2,1)}(x,y) + 3\bar{c}_y^{(2,1)}(x,y) + 3\bar{c}_y^{(2
       8\bar{c}_{x}^{(3,0)}(x,y) + 2\bar{c}_{y}^{(3,0)}(x,y)) + \bar{c}_{x}(x,y)(\bar{c}_{y}^{(0,1)}(x,y)(4\bar{c}_{x}^{(0,3)}(x,y) + 16\bar{c}_{y}^{(0,3)}(x,y) + 6\bar{c}_{x}^{(1,2)}(x,y) + 2\bar{c}_{y}^{(1,2)}(x,y) + 6\bar{c}_{x}^{(2,1)}(x,y) + 6\bar{c}_
4\bar{c}_{\nu}^{(2,1)}(x,y) + \bar{c}_{x}^{(3,0)}(x,y)) - 2\bar{c}_{y}(x,y)(\bar{c}_{x}^{(0,4)}(x,y) + 5\bar{c}_{\nu}^{(0,4)}(x,y) + 2\bar{c}_{x}^{(1,3)}(x,y) + \bar{c}_{\nu}^{(1,3)}(x,y) + 3\bar{c}_{x}^{(2,2)}(x,y) + 3\bar{c}_{\nu}^{(2,2)}(x,y) + 3\bar{c}_
\bar{c}_{x}^{(3,1)}(x,y) + 2\bar{c}_{y}^{(3,1)}(x,y) + 5\bar{c}_{x}^{(4,0)}(x,y) + \bar{c}_{y}^{(4,0)}(x,y)))],
k_{4,2} = \frac{\bar{c}_x(x,y)(\bar{c}_y(x,y)(\bar{c}_x^{(0,4)}(x,y) + 3\bar{c}_x^{(2,2)}(x,y) + 5\bar{c}_x^{(4,0)}(x,y)) - \bar{c}_y^{(0,1)}(x,y)(2\bar{c}_x^{(0,3)}(x,y) + 3\bar{c}_x^{(2,1)}(x,y))) - 2\bar{c}_y(x,y)\bar{c}_x^{(1,0)}(x,y)(\bar{c}_x^{(1,2)}(x,y) + 4\bar{c}_x^{(3,0)}(x,y))}{240\bar{c}_x(x,y)\bar{c}_y(x,y)(\bar{c}_x(x,y) + \bar{c}_y(x,y))},
k_{4,3} = \frac{1}{960\bar{c}_x(x,y)\bar{c}_y(x,y)(\bar{c}_x(x,y) + \bar{c}_y(x,y))} [\bar{c}_y(x,y)\bar{c}_x^{(1,0)}(x,y) - \bar{c}_y^{(0,3)}(x,y) + 4\bar{c}_x^{(1,2)}(x,y) + 6\bar{c}_y^{(1,2)}(x,y) - 2\bar{c}_x^{(2,1)}(x,y) - 6\bar{c}_y^{(2,1)}(x,y) + 4\bar{c}_y^{(1,2)}(x,y) + 4\bar{c}_y^{(
   16\bar{c}_{x}^{(3,0)}(x,y) + 4\bar{c}_{y}^{(3,0)}(x,y)) + \bar{c}_{x}(x,y)(\bar{c}_{y}^{(0,1)}(x,y)(4\bar{c}_{x}^{(0,3)}(x,y) + 16\bar{c}_{y}^{(0,3)}(x,y) - 6\bar{c}_{x}^{(1,2)}(x,y) - 2\bar{c}_{y}^{(1,2)}(x,y) + 6\bar{c}_{x}^{(2,1)}(x,y) + 6\bar{c}_{y}^{(2,1)}(x,y) + 6\bar{c}
4\bar{c}_{v}^{(2,1)}(x,y) - \bar{c}_{x}^{(3,0)}(x,y)) - 2\bar{c}_{y}(x,y)(\bar{c}_{x}^{(0,4)}(x,y) + 5\bar{c}_{v}^{(0,4)}(x,y) - 2\bar{c}_{x}^{(1,3)}(x,y) - \bar{c}_{v}^{(1,3)}(x,y) + 3\bar{c}_{x}^{(2,2)}(x,y) + 3\bar{c}_{v}^{(2,2)}(x,y) - 2\bar{c}_{x}^{(1,3)}(x,y) + 3\bar{c}_{x}^{(2,2)}(x,y) + 3\bar{c}_{x}^{(2,2)}(x,y) + 3\bar{c}_{y}^{(2,2)}(x,y) + 3\bar{c}_
\bar{c}_{x}^{(3,1)}(x,\,y) - 2\bar{c}_{y}^{(3,1)}(x,\,y) + 5\bar{c}_{x}^{(4,0)}(x,\,y) + \bar{c}_{y}^{(4,0)}(x,\,y)))],
                                                                                   \underline{\bar{c}_x(x,y)}(\bar{c}_y(x,y)(5\bar{c}_y^{(0,4)}(x,y)+3\bar{c}_y^{(2,2)}(x,y)+\bar{c}_y^{(4,0)}(x,y))-2\bar{c}_y^{(0,1)}(x,y)(4\bar{c}_y^{(0,3)}(x,y)+\bar{c}_y^{(2,1)}(x,y)))-\bar{c}_y(x,y)\bar{c}_x^{(1,0)}(x,y)(3\bar{c}_y^{(1,2)}(x,y)+2\bar{c}_y^{(3,0)}(x,y))
                                                                                                                                                                                                                                                                                                                                                                                                                                                                                                                                                                                                                                                                                                                                                              240\bar{c}_x(x,y)\bar{c}_y(x,y)(\bar{c}_x(x,y)+\bar{c}_y(x,y))
                                                                                                                              k_{4,6} = \frac{\bar{c}_x(x,y)(\bar{c}_y(x,y)(5\bar{c}_y^{(0,4)}(x,y) + 3\bar{c}_y^{(2,2)}(x,y) + \bar{c}_y^{(4,0)}(x,y)) - 2\bar{c}_y^{(0,1)}(x,y)(4\bar{c}_y^{(0,3)}(x,y) + \bar{c}_y^{(2,1)}(x,y))) - \bar{c}_y(x,y)\bar{c}_x^{(1,0)}(x,y)(3\bar{c}_y^{(1,0)}(x,y) + 2\bar{c}_y^{(3,0)}(x,y))}{240\bar{c}_x(x,y)\bar{c}_y(x,y)(\bar{c}_x(x,y) + \bar{c}_y(x,y))},
k_{4,7} = \frac{1}{960\bar{c}_x(x,y)\bar{c}_y(x,y)(\bar{c}_x(x,y) + \bar{c}_y(x,y))} [\bar{c}_y(x,y)\bar{c}_x^{(1,0)}(x,y) - \bar{c}_y^{(0,3)}(x,y) + 4\bar{c}_x^{(1,2)}(x,y) + 6\bar{c}_y^{(1,2)}(x,y) - 2\bar{c}_x^{(2,1)}(x,y) - 6\bar{c}_y^{(2,1)}(x,y) + 4\bar{c}_y^{(1,2)}(x,y) + 6\bar{c}_y^{(1,2)}(x,y) + 6\bar{c}_y^{(
       16\bar{c}_{v}^{(3,0)}(x,y) + 4\bar{c}_{v}^{(3,0)}(x,y)) + \bar{c}_{x}(x,y)(\bar{c}_{v}^{(0,1)}(x,y)(4\bar{c}_{v}^{(0,3)}(x,y) + 16\bar{c}_{v}^{(0,3)}(x,y) - 6\bar{c}_{v}^{(1,2)}(x,y) - 2\bar{c}_{v}^{(1,2)}(x,y) + 6\bar{c}_{v}^{(2,1)}(x,y) + 6\bar{c}
4\bar{c}_{v}^{(2,1)}(x,y) - \bar{c}_{x}^{(3,0)}(x,y)) - 2\bar{c}_{y}(x,y)(\bar{c}_{x}^{(0,4)}(x,y) + 5\bar{c}_{v}^{(0,4)}(x,y) - 2\bar{c}_{x}^{(1,3)}(x,y) - \bar{c}_{v}^{(1,3)}(x,y) + 3\bar{c}_{x}^{(2,2)}(x,y) + 3\bar{c}_{v}^{(2,2)}(x,y) - 2\bar{c}_{y}^{(1,3)}(x,y) + 3\bar{c}_{y}^{(2,2)}(x,y) + 3\bar{c}_
\bar{c}_{x}^{(3,1)}(x,\,y) - 2\bar{c}_{y}^{(3,1)}(x,\,y) + 5\bar{c}_{x}^{(4,0)}(x,\,y) + \bar{c}_{y}^{(4,0)}(x,\,y)))],
                                                                                   \frac{\bar{c}_x(x,y)(\bar{c}_y(x,y)(\bar{c}_x^{(0,4)}(x,y)+3\bar{c}_x^{(2,2)}(x,y)+5\bar{c}_x^{(4,0)}(x,y))-\bar{c}_y^{(0,1)}(x,y)(2\bar{c}_x^{(0,3)}(x,y)+3\bar{c}_x^{(2,1)}(x,y)))-2\bar{c}_y(x,y)\bar{c}_x^{(1,0)}(x,y)(\bar{c}_x^{(1,2)}(x,y)+4\bar{c}_x^{(3,0)}(x,y))}{240\bar{c}_x(x,y)\bar{c}_y(x,y)(\bar{c}_x(x,y)+\bar{c}_y(x,y))}
k_{4,9} = \frac{1}{960\bar{c}_x(x,y)\bar{c}_y(x,y)(\bar{c}_r(x,y) + \bar{c}_y(x,y))} [\bar{c}_y(x,y)\bar{c}_x^{(1,0)}(x,y)(\bar{c}_y^{(0,3)}(x,y) + 2(2\bar{c}_x^{(1,2)}(x,y) + 3\bar{c}_y^{(1,2)}(x,y) + \bar{c}_x^{(2,1)}(x,y) + 3\bar{c}_y^{(2,1)}(x,y) + 3\bar{c}_y^{(2
       8\bar{c}_{x}^{(3,0)}(x,y) + 2\bar{c}_{y}^{(3,0)}(x,y)) + \bar{c}_{x}(x,y)(\bar{c}_{y}^{(0,1)}(x,y)(4\bar{c}_{x}^{(0,3)}(x,y) + 16\bar{c}_{y}^{(0,3)}(x,y) + 6\bar{c}_{x}^{(1,2)}(x,y) + 2\bar{c}_{y}^{(1,2)}(x,y) + 6\bar{c}_{x}^{(2,1)}(x,y) + 6\bar{c}_{y}^{(2,1)}(x,y) + 6\bar{c}_
   4\bar{c}_{v}^{(2,1)}(x,y) + \bar{c}_{x}^{(3,0)}(x,y)) - 2\bar{c}_{y}(x,y)(\bar{c}_{x}^{(0,4)}(x,y) + 5\bar{c}_{v}^{(0,4)}(x,y) + 2\bar{c}_{x}^{(1,3)}(x,y) + \bar{c}_{v}^{(1,3)}(x,y) + 3\bar{c}_{v}^{(2,2)}(x,y) + 3\bar{c}_
\bar{c}_{x}^{(3,1)}(x,y) + 2\bar{c}_{y}^{(3,1)}(x,y) + 5\bar{c}_{x}^{(4,0)}(x,y) + \bar{c}_{y}^{(4,0)}(x,y)))]
```

These coefficients provide the following local truncation error in Eq. (14):

$$\begin{split} e &= \frac{h^6}{1200\bar{c}_x\bar{c}_y(\bar{c}_x + \bar{c}_y)} [\bar{c}_x(-\bar{c}_y^{(0,1)}(10\bar{c}_x^{(1,3)}u_5^{(1,0)} + 5\bar{c}_x^{(1,1)}u_5^{(3,0)} + 5\bar{c}_x^{(3,1)}u_5^{(1,0)} + 5\bar{c}_x^{(1,0)}u_5^{(3,1)} + 50\bar{c}_y^{(0,2)}u_5^{(0,3)} \\ &+ 5\bar{c}_y^{(2,0)}u_5^{(0,3)} + 10\bar{c}_y^{(1,0)}u_5^{(1,3)} + 5(2\bar{c}_y^{(0,4)} + \bar{c}_y^{(2,2)})u_5^{(0,1)} - 9\bar{c}_yu_5^{(0,5)}) + \bar{c}_y(5\bar{c}_x^{(1,4)}u_5^{(1,0)} - 75\bar{c}_x^{(2,0)}u_5^{(2,2)} \\ &+ 5\bar{c}_x^{(1,2)}u_5^{(3,0)} + 40\bar{c}_x^{(3,0)}u_5^{(3,0)} + 10\bar{c}_x^{(1,1)}u_5^{(3,1)} + 5\bar{c}_x^{(3,2)}u_5^{(1,0)} + 35\bar{c}_x^{(2,0)}u_5^{(4,0)} + 5\bar{c}_x^{(5,0)}u_5^{(1,0)} + 9\bar{c}_x^{(1,0)}u_5^{(5,0)} \\ &+ 40\bar{c}_y^{(0,3)}u_5^{(0,3)} + 5\bar{c}_y^{(2,1)}u_5^{(0,3)} + 5\bar{c}_y^{(0,5)}u_5^{(0,1)} + 10\bar{c}_y^{(1,1)}u_5^{(1,3)} + 5\bar{c}_y^{(0,2)}(7u_5^{(0,4)} - 15u_5^{(2,2)}) + 5\bar{c}_y^{(2,3)}u_5^{(0,1)} \\ &+ 5\bar{c}_y^{(4,1)}u_5^{(0,1)} + 3\bar{c}_yu_5^{(0,6)}) + (\bar{c}_y^{(0,1)})^2(50u_5^{(2,2)} - 30u_5^{(0,4)})) - 5\bar{c}_x^{(1,0)}\bar{c}_y(\bar{c}_x^{(2,2)}u_5^{(1,0)} - 10\bar{c}_x^{(1,0)}u_5^{(2,2)} \\ &+ \bar{c}_x^{(0,2)}u_5^{(3,0)} + 10\bar{c}_x^{(2,0)}u_5^{(3,0)} + 2\bar{c}_x^{(0,1)}u_5^{(3,1)} + 2\bar{c}_x^{(4,0)}u_5^{(1,0)} + 6\bar{c}_x^{(1,0)}u_5^{(4,0)} + \bar{c}_y^{(1,1)}u_5^{(0,3)} + \bar{c}_y^{(0,1)}u_5^{(3,1)} \\ &+ (\bar{c}_y^{(1,3)} + 2\bar{c}_y^{(3,1)})u_5^{(0,1)}) + 3\bar{c}_x^2\bar{c}_yu_5^{(6,0)}] + O(h^7) \end{split}$$

# Appendix C. The explicit expression for the term $\bar{f}_5$ in Eq. (20) in the case of nonzero loading (source) term $f \neq 0$ in the wave (heat) equation

The expression for  $\bar{f}_5$  up to the sixth order with respect to h:

$$\begin{split} \bar{f}_5 &= \mathbf{h}^2 f_5(m_{0,1} + m_{0,2} + m_{0,3} + m_{0,4} + m_{0,5} + m_{0,6} + m_{0,7} + m_{0,8} + m_{0,9}) \\ &+ \mathbf{h}^3 (f_5^{(0,1)}(-d_1 m_{0,1} - d_2 m_{0,2} - d_3 m_{0,3} + d_6 m_{0,7} + d_7 m_{0,8} + d_8 m_{0,9}) + f_5^{(1,0)}(-d_1 m_{0,1} + d_3 m_{0,3} \\ &- d_4 m_{0,4} + d_5 m_{0,6} - d_6 m_{0,7} + d_8 m_{0,9}) + f_5(m_{1,1} + m_{1,2} + m_{1,3} + m_{1,4} + m_{1,5} + m_{1,6} + m_{1,7} \\ &+ m_{1,8} + m_{1,9})) + \frac{1}{2} \mathbf{h}^4 (f_5^{(0,2)}(d_1^2 m_{0,1} + d_2^2 m_{0,2} + d_3^2 m_{0,3} + d_6^2 m_{0,7} + d_7^2 m_{0,8} + d_8^2 m_{0,9}) \\ &+ 2d_1^2 m_{0,1} f_5^{(1,1)} + d_1^2 m_{0,1} f_5^{(2,0)} - 2f_5^{(0,1)}(d_1 m_{1,1} + d_2 m_{1,2} + d_3 m_{1,3} - d_6 m_{1,7} - d_7 m_{1,8} - d_8 m_{1,9}) \\ &- 2d_1 m_{1,1} f_5^{(1,0)} - 2d_3^2 m_{0,3} f_5^{(1,1)} + d_3^2 m_{0,3} f_5^{(2,0)} + 2d_3 m_{1,3} f_5^{(1,0)} + d_4^2 m_{0,4} f_5^{(2,0)} - 2d_4 m_{1,4} f_5^{(1,0)} \end{split}$$

$$+ d_5^2 m_{0,6} f_5^{(2,0)} + 2 d_5 m_{1,6} f_5^{(1,0)} - 2 d_6^2 m_{0,7} f_5^{(1,1)} + d_6^2 m_{0,7} f_5^{(2,0)} - 2 d_6 m_{1,7} f_5^{(1,0)} + 2 d_8^2 m_{0,9} f_5^{(1,1)} \\ + d_8^2 m_{0,9} f_5^{(2,0)} + 2 d_8 m_{1,9} f_5^{(1,0)} + \frac{1}{6} \mathbf{h}^5 (f_5^{(0,3)} (d_1^3 (-m_{0,1}) - d_2^3 m_{0,2} - d_3^3 m_{0,3} + d_6^3 m_{0,7} \\ + d_7^2 m_{0,8} + d_8^3 m_{0,9}) - 3 d_1^3 m_{0,1} f_5^{(1,2)} - 3 d_1^3 m_{0,1} f_5^{(2,1)} - d_1^3 m_{0,1} f_5^{(3,0)} + 3 f_5^{(0,2)} (d_1^2 m_{1,1} + d_2^2 m_{1,2} \\ + d_3^2 m_{1,3} + d_6^2 m_{1,7} + d_7^2 m_{1,8} + d_8^2 m_{1,9}) + 6 d_1^2 m_{1,1} f_5^{(1,1)} + 3 d_1^2 m_{1,1} f_5^{(2,0)} + 3 d_3^3 m_{0,3} f_5^{(1,2)} \\ - 3 d_3^3 m_{0,3} f_5^{(2,1)} + d_3^3 m_{0,3} f_5^{(3,0)} - 6 d_3^2 m_{1,3} f_5^{(1,1)} + 3 d_3^2 m_{1,3} f_5^{(2,0)} - d_4^3 m_{0,4} f_5^{(3,0)} + 3 d_4^2 m_{1,4} f_5^{(2,0)} \\ + d_5^2 m_{0,6} f_5^{(3,0)} + 3 d_5^2 m_{1,6} f_5^{(2,0)} - 3 d_6^3 m_{0,7} f_5^{(1,2)} + 3 d_6^3 m_{0,7} f_5^{(2,1)} - d_6^3 m_{0,7} f_5^{(3,0)} - 6 d_6^2 m_{1,7} f_5^{(1,1)} \\ + 3 d_6^2 m_{1,7} f_5^{(2,0)} + 3 d_8^3 m_{0,9} f_5^{(1,2)} + 3 d_8^3 m_{0,9} f_5^{(2,1)} + d_8^3 m_{0,9} f_5^{(3,0)} + 6 d_8^2 m_{1,9} f_5^{(1,1)} + 3 d_8^2 m_{1,9} f_5^{(2,0)} \\ + \frac{1}{24} \mathbf{h}^6 (f_5^{(0,4)} (d_1^4 m_{0,1} + d_2^4 m_{0,2} + d_3^4 m_{0,3} + d_6^4 m_{0,7} + d_7^4 m_{0,8} + d_8^4 m_{0,9}) + 4 d_1^4 m_{0,1} f_5^{(1,2)} \\ + 6 d_1^4 m_{0,1} f_5^{(2,2)} + 4 d_1^4 m_{0,1} f_5^{(3,1)} + d_1^4 m_{0,1} f_5^{(4,0)} - 4 f_5^{(0,3)} (d_1^3 m_{1,1} + d_2^3 m_{1,2} + d_3^3 m_{1,3} - d_6^3 m_{1,7} \\ - d_7^3 m_{1,8} - d_8^3 m_{1,9}) - 12 d_1^3 m_{1,1} f_5^{(1,2)} - 12 d_1^3 m_{1,1} f_5^{(2,1)} - 4 d_1^3 m_{1,1} f_5^{(3,0)} - 4 d_1^4 m_{0,1} f_5^{(3,0)} \\ + 6 d_4^4 m_{0,3} f_5^{(2,2)} - 4 d_3^4 m_{0,3} f_5^{(4,0)} + 12 d_3^3 m_{1,3} f_5^{(1,2)} - 12 d_3^3 m_{1,3} f_5^{(2,1)} + 4 d_3^3 m_{1,3} f_5^{(2,1)} + 4 d_3^3 m_{1,3} f_5^{(2,1)} \\ + d_4^4 m_{0,4} f_5^{(4,0)} - 4 d_4^4 m_{0,5} f_5^{(4,0)} - 12 d_6^3 m_{1,7} f_5^{(1,2)} + 12 d_6^3 m_{1,7} f_5^{(2,1)} - 4 d_6^3 m_{1,7} f_5^{(3,0)} + 4 d_8^4 m_{0,9} f_5^{(3,1)} + d$$

## Appendix D. Supplementary data

Supplementary material related to this article can be found online at https://doi.org/10.1016/j.cma.2020.113249.

#### References

- [1] H. Ahmadian, M. Friswell, J. Mottershead, Minimization of the discretization error in mass and stiffness formulations by an inverse method, Internat. J. Numer. Methods Engrg. 41 (2) (1998) 371–387.
- [2] M. Ainsworth, H.A. Wajid, Optimally blended spectral-finite element scheme for wave propagation and nonstandard reduced integration, SIAM J. Numer. Anal. 48 (1) (2010) 346–371.
- [3] H.P. Cherukuri, Dispersion analysis of numerical approximations to plane wave motions in an isotropic elastic solid, Comput. Mech. 25 (4) (2000) 317–328.
- [4] W. Dauksher, A.F. Emery, Solution of elastostatic and elastodynamic problems with Chebyshev spectral finite elements, Comput. Methods Appl. Mech. Engrg. 188 (1) (2000) 217–233.
- [5] D. Gabriel, J. Plesek, R. Kolman, F. Vales, Dispersion of elastic waves in the contact-impact problem of a long cylinder, J. Comput. Appl. Math. 234 (2010) 1930–1936.
- [6] M.N. Guddati, B. Yue, Modified integration rules for reducing dispersion error in finite element method, Comput. Methods Appl. Mech. Engrg. 193 (2004) 275–287.
- [7] V. Gyrya, K. Lipnikov, M-adaptation method for acoustic wave equation on square meshes, J. Comput. Acoust. 20 (2012) 1250022–1:23.
- [8] S. Krenk, Dispersion-corrected explicit integration of the wave equation, Comput. Methods Appl. Mech. Engrg. 191 (2001) 975–987.
- [9] K.J. Marfurt, Accuracy of finite difference and finite element modeling of the scalar and elastic wave equation, Geophysics 49 (1984) 533–549.
- [10] R. Mullen, T. Belytschko, Dispersion analysis of finite element semidiscretizations of the two-dimensional wave equation, Internat. J. Numer. Methods Engrg. 18 (1982) 11–29.
- [11] G. Seriani, S.P. Oliveira, Optimal blended spectral-element operators for acoustic wave modeling, Geophysics 72 (5) (2007) 95–106.
- [12] G. Seriani, S.P. Oliveira, Dispersion analysis of spectral element methods for elastic wave propagation, Wave Motion 45 (6) (2008) 729–744.
- [13] B. Yue, M.N. Guddati, Dispersion-reducing finite elements for transient acoustics, J. Acoust. Soc. Am. 118 (4) (2005) 2132–2141.
- [14] F.I. Zyserman, P.M. Gauzellino, Dispersion analysis of a nonconforming finite element method for the three-dimensional scalar and elastic wave equations, Finite Elem. Anal. Des. 41 (13) (2005) 1309–1326.
- [15] T. Hughes, A. Reali, G. Sangalli, Duality and unified analysis of discrete approximations in structural dynamics and wave propagation: Comparison of p-method finite elements with k-method nurbs, Comput. Methods Appl. Mech. Engrg. 197 (49–50) (2008) 4104–4124.
- [16] X. Li, T. Zhu, M. Zhang, G. Long, Seismic scalar wave equation with variable coefficients modeling by a new convolutional differentiator, Comput. Phys. Comm. 181 (11) (2010) 1850–1858.

- [17] Z.C. He, A.G. Cheng, G.Y. Zhang, Z.H. Zhong, G.R. Liu, Dispersion error reduction for acoustic problems using the edge-based smoothed finite element method (es-fem), Internat. J. Numer. Methods Engrg. 86 (11) (2011) 1322–1338.
- [18] D. Wang, R. Tezaur, J. Toivanen, C. Farhat, Overview of the discontinuous enrichment method, the ultra-weak variational formulation, and the partition of unity method for acoustic scattering in the medium frequency regime and performance comparisons, Internat. J. Numer. Methods Engrg. 89 (4) (2012) 403–417.
- [19] D. Wang, W. Liu, H. Zhang, Novel higher order mass matrices for isogeometric structural vibration analysis, Comput. Methods Appl. Mech. Engrg. 260 (2013) 92–108.
- [20] D. Wang, W. Liu, H. Zhang, Superconvergent isogeometric free vibration analysis of Euler-Bernoulli beams and kirchhoff plates with new higher order mass matrices, Comput. Methods Appl. Mech. Engrg. 286 (2015) 230–267.
- [21] A. Idesman, M. Schmidt, J.R. Foley, Accurate finite element modeling of linear elastodynamics problems with the reduced dispersion error, Comput. Mech. 47 (2011) 555–572.
- [22] A.V. Idesman, D. Pham, Finite element modeling of linear elastodynamics problems with explicit time-integration methods and linear elements with the reduced dispersion error, Comput. Methods Appl. Mech. Engrg. 271 (2014) 86–108.
- [23] A.V. Idesman, D. Pham, Accurate finite element modeling of acoustic waves, Comput. Phys. Comm. 185 (2014) 2034–2045.
- [24] A. Idesman, Optimal reduction of numerical dispersion for wave propagation problems. part 1: Application to 1-d isogeometric elements, Comput. Methods Appl. Mech. Engrg. 317 (2017) 970–992.
- [25] A. Idesman, B. Dey, Optimal reduction of numerical dispersion for wave propagation problems. part 2: Application to 2-d isogeometric elements, Comput. Methods Appl. Mech. Engrg. 321 (2017) 235–268.
- [26] A. Idesman, B. Dey, The use of the local truncation error for the increase in accuracy of the linear finite elements for heat transfer problems, Comput. Methods Appl. Mech. Engrg. 319 (2017) 52–82.
- [27] A. Idesman, B. Dey, New 25-point stencils with optimal accuracy for 2-d heat transfer problems. Comparison with the quadratic isogeometric elements, J. Comput. Phys. 418 (2020) 109640.
- [28] A. Idesman, The use of the local truncation error to improve arbitrary-order finite elements for the linear wave and heat equations, Comput. Methods Appl. Mech. Engrg. 334 (2018) 268–312.
- [29] K. Singh, J. Williams, A parallel fictitious domain multigrid preconditioner for the solution of poisson's equation in complex geometries, Comput. Methods Appl. Mech. Engrg. 194 (4547) (2005) 4845–4860.
- [30] P. Vos, R. van Loon, S. Sherwin, A comparison of fictitious domain methods appropriate for spectral/hp element discretisations, Comput. Methods Appl. Mech. Engrg. 197 (2528) (2008) 2275–2289.
- [31] E. Burman, P. Hansbo, Fictitious domain finite element methods using cut elements: I. a stabilized Lagrange multiplier method, Comput. Methods Appl. Mech. Engrg. 199 (4144) (2010) 2680–2686.
- [32] E. Rank, S. Kollmannsberger, C. Sorger, A. Duster, Shell finite cell method: A high order fictitious domain approach for thin-walled structures, Comput. Methods Appl. Mech. Engrg. 200 (45–46) (2011) 3200–3209.
- [33] E. Rank, M. Ruess, S. Kollmannsberger, D. Schillinger, A. Duster, Geometric modeling, isogeometric analysis and the finite cell method, Comput. Methods Appl. Mech. Engrg. 249–252 (2012) 104–115.
- [34] T. Fries, S. Omerovi, D. Schllhammer, J. Steidl, Higher-order meshing of implicit geometries—part i: Integration and interpolation in cut elements, Comput. Methods Appl. Mech. Engrg. 313 (2017) 759–784.
- [35] T. Hoang, C.V. Verhoosel, F. Auricchio, E.H. van Brummelen, A. Reali, Mixed isogeometric finite cell methods for the Stokes problem, Comput. Methods Appl. Mech. Engrg. 316 (2017) 400–423.
- [36] S. Zhao, G.W. Wei, Matched interface and boundary (mib) for the implementation of boundary conditions in high-order central finite differences, Internat. J. Numer. Methods Engrg. 77 (12) (2009) 1690–1730.
- [37] S. May, M. Berger, An explicit implicit scheme for cut cells in embedded boundary meshes, J. Sci. Comput. 71 (3) (2017) 919-943.
- [38] H.-O. Kreisst, N.A. Petersson, An embedded boundary method for the wave equation with discontinuous coefficients, SIAM J. Sci. Comput. 28 (6) (2006) 2054–2074.
- [39] H.-O. Kreiss, N.A. Petersson, A second order accurate embedded boundary method for the wave equation with Dirichlet data, SIAM J. Sci. Comput. 27 (4) (2006) 1141–1167.
- [40] H.-O. Kreiss, N.A. Petersson, J. Ystrom, Difference approximations of the Neumann problem for the second order wave equation, SIAM J. Numer. Anal. 42 (3) (2004) 1292–1323.
- [41] Z. Jomaa, C. Macaskill, The shortley-weller embedded finite-difference method for the 3d poisson equation with mixed boundary conditions, J. Comput. Phys. 229 (10) (2010) 3675–3690.
- [42] Z. Jomaa, C. Macaskill, The embedded finite difference method for the poisson equation in a domain with an irregular boundary and Dirichlet boundary conditions, J. Comput. Phys. 202 (2) (2005) 488–506.
- [43] J.L. Hellrung Jr., L. Wang, E. Sifakis, J.M. Teran, A second order virtual node method for elliptic problems with interfaces and irregular domains in three dimensions, J. Comput. Phys. 231 (4) (2012) 2015–2048.
- [44] L. Chen, H. Wei, M. Wen, An interface-fitted mesh generator and virtual element methods for elliptic interface problems, J. Comput. Phys. 334 (2017) 327–348.
- [45] J. Bedrossian, J.H. von Brecht, S. Zhu, E. Sifakis, J.M. Teran, A second order virtual node method for elliptic problems with interfaces and irregular domains, J. Comput. Phys. 229 (18) (2010) 6405–6426.
- [46] D.C. Asshcio, J.M. Teran, A second order virtual node algorithm for Stokes flow problems with interfacial forces, discontinuous material properties and irregular domains, J. Comput. Phys. 250 (2013) 77–105.
- [47] K. Mattsson, M. Almquist, A high-order accurate embedded boundary method for first order hyperbolic equations, J. Comput. Phys. 334 (2017) 255–279.
- [48] P. Schwartz, M. Barad, P. Colella, T. Ligocki, A cartesian grid embedded boundary method for the heat equation and poisson's equation in three dimensions, J. Comput. Phys. 211 (2) (2006) 531–550.

- [49] G. Dakin, B. Despres, S. Jaouen, Inverse lax-wendroff boundary treatment for compressible Lagrange-remap hydrodynamics on Cartesian grids, J. Comput. Phys. 353 (2018) 228–257.
- [50] P. Colella, D.T. Graves, B.J. Keen, D. Modiano, A Cartesian grid embedded boundary method for hyperbolic conservation laws, J. Comput. Phys. 211 (1) (2006) 347–366.
- [51] R. Crockett, P. Colella, D. Graves, A Cartesian grid embedded boundary method for solving the poisson and heat equations with discontinuous coefficients in three dimensions, J. Comput. Phys. 230 (7) (2011) 2451–2469.
- [52] P. McCorquodale, P. Colella, H. Johansen, A Cartesian grid embedded boundary method for the heat equation on irregular domains, J. Comput. Phys. 173 (2) (2001) 620–635.
- [53] H. Johansen, P. Colella, A Cartesian grid embedded boundary method for poisson's equation on irregular domains, J. Comput. Phys. 147 (1) (1998) 60–85.
- [54] J.B. Angel, J.W. Banks, W.D. Henshaw, High-order upwind schemes for the wave equation on overlapping grids: Maxwell's equations in second-order form, J. Comput. Phys. 352 (2018) 534–567.
- [55] H. Uddin, R. Kramer, C. Pantano, A Cartesian-based embedded geometry technique with adaptive high-order finite differences for compressible flow around complex geometries, J. Comput. Phys. 262 (2014) 379–407.
- [56] A. Main, G. Scovazzi, The shifted boundary method for embedded domain computations. part i: poisson and Stokes problems, J. Comput. Phys. (2017).
- [57] T. Song, A. Main, G. Scovazzi, M. Ricchiuto, The shifted boundary method for hyperbolic systems: Embedded domain computations of linear waves and shallow water flows, J. Comput. Phys. 369 (2018) 45–79.
- [58] S. Hosseinverdi, H.F. Fasel, An efficient, high-order method for solving Poisson equation for immersed boundaries: Combination of compact difference and multiscale multigrid methods, J. Comput. Phys. 374 (2018) 912–940.
- [59] S. Britt, S. Tsynkov, E. Turkel, Numerical solution of the wave equation with variable wave speed on nonconforming domains by high-order difference potentials, J. Comput. Phys. 354 (2018) 26–42.
- [60] K. Swaminathan, D. Sangeetha, Thermal analysis of fgm plates a critical review of various modeling techniques and solution methods, Compos. Struct. 160 (2017) 43–60.
- [61] A. Idesman, A new numerical approach to the solution of PDEs with optimal accuracy on irregular domains and cartesian meshes. part 1: the derivations for the wave, heat and poisson equations in the 1-d and 2-d cases., Arch. Appl. Mech. (2020) 1–35, submitted for publication.
- [62] B. Dey, A. Idesman, A new numerical approach to the solution of PDEs with optimal accuracy on irregular domains and Cartesian meshes, part 2: numerical simulation and comparison with FEM., Arch. Appl. Mech. (2020) 1 32, submitted for publication.
- [63] A. Idesman, B. Dey, A new 3-d numerical approach to the solution of PDEs with optimal accuracy on irregular domains and Cartesian meshes, Comput. Methods Appl. Mech. Engrg. 354 (2019) 568–592.
- [64] A. Idesman, B. Dey, Compact high-order stencils with optimal accuracy for numerical solutions of 2-D time-independent elasticity equations, Comput. Methods Appl. Mech. Engrg. 360 (2020) 112699.
- [65] A. Idesman, B. Dey, Accurate numerical solutions of 2-D elastodynamics problems using compact high-order stencils., Comput. Struct. 229 (2020) 106160.
- [66] A. Idesman, B. Dey, A new numerical approach to the solution of the 2-D Helmholtz equation with optimal accuracy on irregular domains and Cartesian meshes, Comput. Mech. 65 (2020) 1189–1204.
- [67] Wolfram Research, Inc., Mathematica, Version 12.0, URL https://www.wolfram.com/mathematica.
- [68] B. Szabo, I. Babuska, Finite Element Analysis, Wiley, New York, 1991.
- [69] COMSOL AB, Stockholm, Sweden, COMSOL Multiphysics, Version 3.5, URL https://www.comsol.com.
- [70] K. Salari, P. Knupp, Code verification by the method of manufactured solutions, in: Sandia Report, SAND 2000-1444, Sandia National Laboratories, Albuquerque, NM, 2000, pp. 1–124.